Utrecht University

MSc thesis

The Influence of Glacial Lake Development on Glacier Flow Velocities and Thinning Rates in the Bhutanese Himalayas

MSc Earth Surface and Water
Utrecht University

Author:

Jan Ædzer Hellema

6508316

Supervisors:

Faezeh Maghami Nick

Walter Immerzeel

Date:

26/01/2024

Abstract

Mountain glaciers in High Mountain Asia have experienced rapid shrinking and thinning in recent decades through global warming. In addition, more and more glaciers are developing massive lakes at their front, mainly forming in overdeepenings as glaciers retreat. These proglacial lakes have the ability to rapidly accelerate glacier melt as glaciers actively calve into the lake. The formation and expansion of these proglacial lakes heavily affect downstream regions as the water supply is reduced, and the risk for glacial lake outburst floods (GLOFs) increases. It is therefore crucial to study the development of these glacial lakes and to increase our understanding of the influence that these lakes exert on glacier dynamics. This study shows how glacial lake development has affected glacier flow velocities and thinning rates in the Bhutanese Lunana region over the past two decades. Five glaciers were selected from this region, among which one land-terminating glacier and four lake-terminating glaciers. The development of the lakes in this region was mapped using Landsat, RapidEye and PlanetScope imagery to calculate the NDWI. By applying a newly developed feature tracking tool, GIV, the flow velocities were derived over five selected periods from the past two decades. The thinning rate and mass loss from 1975 to 2022 were estimated by combining existing data with data obtained from DEM differencing. The results showed that the glacial lakes have experienced rapid expansion over the past two decades, heavily affecting the flow velocity and thinning rates of glaciers. Some lake-terminating glaciers in the region were characterized by significantly higher flow velocities and thinning rates, mainly at the glacier front compared to land-terminating glaciers, which are mainly influenced by supraglacial lake development and rising air temperatures. The dominant processes at lake-terminating glaciers, causing these high velocities and thinning rates, are dynamic thinning and buoyant uplift which reduce basal stress, causing an acceleration of the terminus and consequently buoyancy-induced calving through a positive feedback. Other lake-terminating glaciers in the region were less affected by their lakes as their fronts were only subjected to subaqueous melt and thermal-notching. For these glaciers, the velocities were decreasing, caused by a decrease in driving stresses by increased glacier thinning. It is estimated that proglacial lakes are likely to expand in the future, and new lakes will form through increased global warming and the presence of large overdeepenings underneath the glaciers. However, many aspects of these lakes, including lake bathymetry and temperature, remain unknown, while playing an important role in glacier-lake interactions. Therefore, additional research and fieldwork is needed to obtain crucial information necessary to study and understand these complex processes. In addition, the risks GLOFs in mountainous regions increase, highlighting the importance for further research to safeguard downstream communities.

Table of contents

1. Introduction

The continuous rise in temperature and changes in precipitation patterns due to climate change has caused mountain glaciers in High Mountain Asia (HMA) to undergo rapid shrinking and thinning in recent decades [Furian et al., 2021; Gardner et al., 2013; IPCC, 2021]. Between 2000 and 2018, HMA glaciers have lost up to a total of 19 ± 2.5 Gt yr^{-1} or -0.19 ± 0.03 m w.e. yr^{-1} on average [Shean et al., 2020] and might potentially result in a glacier mass loss of up to 87% in HMA at the end of the century [Kraaijenbrink et al., 2017; Hock et al., 2019; Marzeion et al., 2020]. Although most regions experience increased mass loss and decreased flow velocities, some regions still show contrasting results, emphasizing the complexity of the cryosphere and the need for region-specific approaches [Dehecq et al., 2019]. Glacier melt can accelerate even further by the formation and expansion of glacial lakes, both on top of the glacier, and at the termini of retreating glaciers [Benn et al., 2007; Fujita et al., 2009; Haritashya et al., 2018; Komori, 2008; Sato et al., 2022]. Additionally, the area and volume of glacial lakes are expected to increase under climate change [Furian et al., 2022], significantly influenced by overdeepenings in the glacier beds [Furian et al., 2021].

Glacial lakes can be classified into two types: supraglacial lakes and proglacial lakes. Supraglacial lakes form in the ablation zone and grow by coalescence of smaller lakes [Komori, 2008]. When these lakes expand and merge near the glacier terminus, proglacial lakes can form [Benn et al., 2012; Sato et al., 2022], typically dammed by lateral- and terminal moraines [Benn et al., 2012]. Proglacial lakes accelerate glacier melt significantly through calving [Benn et al., 2007; Sakai et al., 2009; Sato et al., 2022]. The formation of proglacial lakes can transform a land-terminating glacier into a lake-terminating glacier if the glacier directly terminates in the lake, leading to decreased basal resistance [Benn et al., 2007; Pronk et al., 2021]. This reduction in basal resistance can lead to a doubling in glacier flow velocity for lake-terminating glaciers compared to land-terminating glaciers across HMA [Pronk et al., 2021]. Between 2000 and 2015, lake-terminating glaciers were responsible for up to 32% of the observed mass loss between 2000 and 2015, while accounting for only 10-15% of the total glacier area in HMA [King et al., 2019].

The increase in glacier mass loss, coupled with the formation of new lakes and expansion of existing lakes can significantly affect downstream regions. Local residents heavily depend on the water supply by glaciers, and should adapt to earlier freshets and reduced streamflow [Kulkarni et al., 2021; Marshall, 2011]. A more direct threat is the increased risk of glacial lake outburst floods (GLOFs), which can happen spontaneously due to moraine failure and can threaten life and infrastructure downstream [Benn et al., 2012; Clague & O'Connor, 2021; Carrivick & Tweed, 2016; Fujita et al., 2009; Furian et al., 2021; Zheng et al., 2021]. Understanding the mechanisms governing glacial lakes is considered important, not only in terms of understanding glacier dynamics, but also for implementation of localized hazard and risk assessments and strategies, as well as for resource management regarding water storage and hydropower production for downstream communities [Farinotti et al., 2019*a*; Furian et al., 2022; Gardelle et al., 2011; Komori, 2008; Tweed & Carrivick, 2015].

Over the last decades, many studies have been conducted on receding glaciers in HMA, and the influence that glacial lakes have on these glaciers. Nevertheless, many challenges remain regarding this field of study, such as the need for extensive and long term research, closely monitored glaciers, improved boundary conditions and parametrization for glacier models, increased spatiotemporal data coverage, avoiding interference from clouds and snowfall in remote sensing, and a better understanding of physical processes (e.g. calving and subaqueous melt) [Benn et al., 2012; Fowler & Ng, 2021; Komori, 2008].

This study will present an inventory on the evolution of glacial lakes in the Lunana region, along with satellite observations on glacier surface flow velocities, thinning rates and corresponding mass loss. The objective of this study is to link the observations in flow velocities and mass loss to the development of glacial lakes over the past 20 years in the Lunana region, and to determine which processes drive the observed changes and patterns. This research therefore focusses on how glacial lakes affect glacier behavior in the Bhutanese Lunana region. To address this, the following sub-questions have been formulated to get a comprehensive understanding of the research topic:

- How have glacial lakes developed over the past 20 years in the Lunana region?
- How do glacial lakes influence glacier flow velocity and thinning rate, and how does this relate to glacier mass loss in the Lunana region?
- Which processes affect the flow velocity and thinning rate of lake-terminating glaciers compared to land-terminating glaciers?

2. Glacial lakes and glacier dynamics

The number and size of glacial lakes have shown significant increases in recent decades across HMA [Shugar et al., 2020; Zheng et al., 2015], and are associated with accelerated glacier mass loss [Benn et al., 2007; King et al., 2019]. This trend is likely to continue upwards in the near future as the global temperature keeps rising [Furian et al., 2022].

The glacial lakes forming on the glacier surface are called supraglacial lakes. The formation is often promoted by a thin debris-cover on a flat surface in the ablation zone of a glacier [Komori, 2008; Pronk et al., 2021]. The presence of a thin layer of debris on the glacier surface lowers the albedo and increases melt by transferring the stored heat from the incoming solar radiation to the ice underneath. Whereas a thicker layer of debris might insulate the ice underneath [Fowler & Ng, 2021]. Studies conducted in HMA by Benn et al. (2012) and Pratap et al. (2015) showed that the middle part of glaciers, with a thin debris cover, showed the highest ablation rate, whereas the lowest part showed less melt due to a thicker debris cover. This can result in a detachment of the lower ablation zone from the upper accumulation zone, where the lower part becomes stagnant due to decreased driving stresses [Quincey et al., 2009; Rowan et al., 2021]. Furthermore, an upward shift of the equilibrium-line altitude (ELA) might also promote the formation of supraglacial lakes at higher elevations (**fig. 1**) [Khadka et al., 2023; Marshall, 2011].

Two types of supraglacial lakes can be identified according to Benn et al. (2001): perched lakes and base-level lakes. Perched lakes are common at elevations situated above the englacial drainage system. They are often limited in growth up to 200 m in diameter due to periodic outflow via a temporary connection to the englacial drainage system [Benn et al., 2001; Röhl, 2008]. Base-level lakes are located at the level where water leaves the glacier and are connected to the englacial drainage system, which can prolong their existence [Röhl, 2008]. These lakes often develop in large supraglacial lakes, due to coalescence of smaller lakes. The presence of base-level lakes can be an indicator for the formation of a proglacial lake in the future [Benn et al., 2012; Sato et al., 2022].

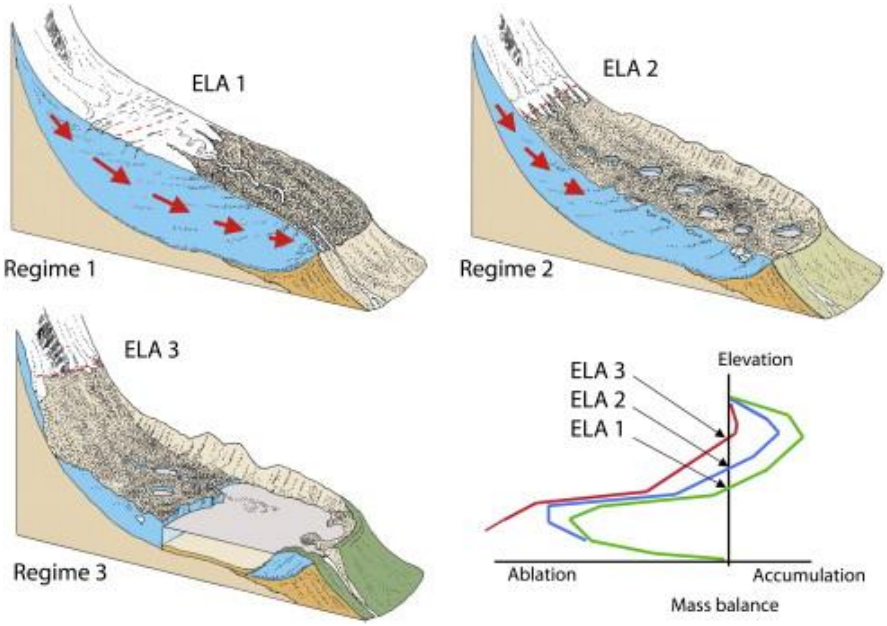

Fig. 1. *Schematic overview of the formation of glacial lakes. Regime 2 shows the appearance of supraglacial lakes, which merge together to form a proglacial lake, which is shown in regime 3. The arrows indicate the flow regime of the glacier. Note how the ELA is shifting upwards, and the effect that it has on the glacier mass balance in the bottom right figure [from Benn et al., 2012].*

The englacial hydraulic system is an important factor for the appearance and drainage of supraglacial lakes. Conduits close over time through the compressive stresses from glacier flow or the blockage by ice or debris. The drainage of warm water, originating from supraglacial lakes, might open these conduits again caused by ablation through frictional heating. Over time, roof collapse due to the enlargement of englacial conduits might occur, creating larger supraglacial lakes, which would enhance mass loss further through a positive feedback loop [Benn et al., 2012; Fowler & Ng, 2021; Sakai et al., 2000]. Lake drainage can also occur through hydrofracturing, where water enters existing crevasses in the ice, enlarging it through frictional heating [Benn et al., 2009].

Besides the collapse of englacial conduits, supraglacial lakes can expand through several processes. Subaerial melt occurs due to the absorption of short wave solar radiation by the ice or debris on the slopes surrounding supraglacial lakes [Röhl, 2008]. On sloping ice faces, the orientation influences subaerial melt significantly where ablation is highest from southeast to southwest facing slopes [Benn et al., 2001]. Since the temperature of the water is higher than the surrounding ice faces, melt occurs at the water-line combined with wind-driven advection (i.e. thermal-notching). This produces notches, which weaken the overlying ice [Gardelle et al., 2011]. Supraglacial lakes can also expand due to the calving of ice blocks in the water. Many factors influence calving, among which water depth, cliff height and the presence of crevasses around the lake leading to hydrofracturing [Benn et al., 2012; Gardelle et al., 2011; Sakai et al., 2009]. Although subaqueous melt or thermal undercutting is often mentioned as a process leading to supraglacial lake expansion, Röhl (2008) argued that the accumulation of debris at the front of the ice cliff halts this mechanism. This occurs unless the water is deep enough for thermal undercutting to be effective, typically observed at the glacier-proglacial lake interface (**fig. 2**).

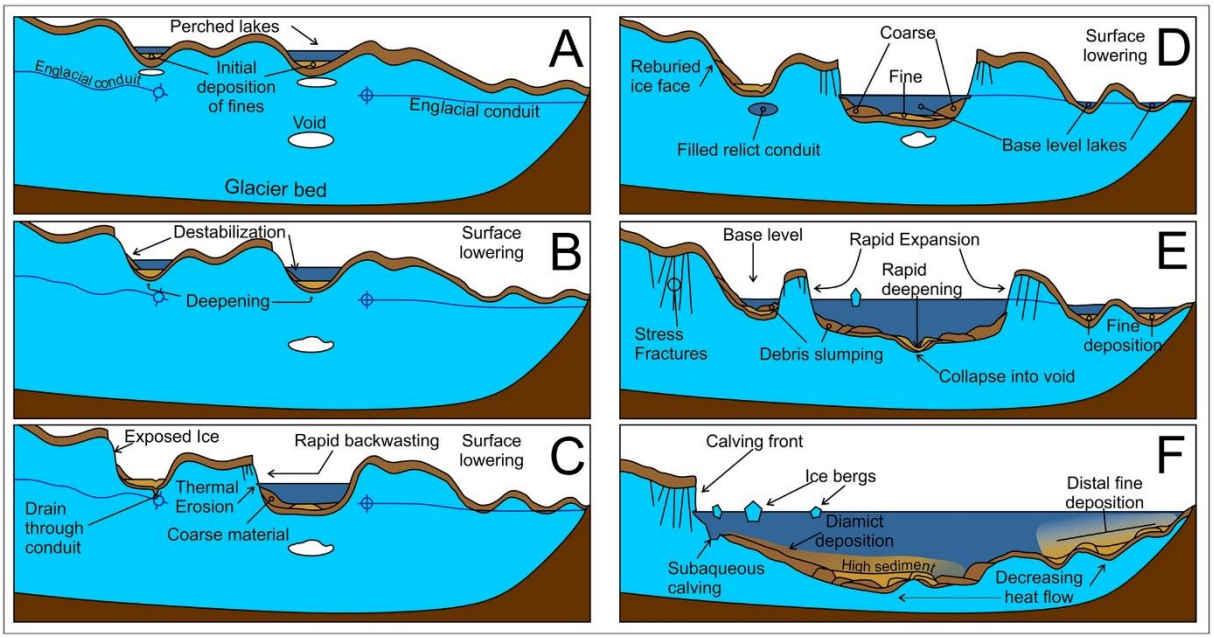

Fig. 2. *Schematic representation showing the development of supraglacial lakes and the transition into a moraine-dammed proglacial lake. In stages a-c, the supraglacial lakes expand and drain through englacial conduits. In stage d-e, the largest lake deepens and connects to a conduit, filling lower lying basins. In f, the continuous deepening and coalescing of smaller lakes has resulted in the formation of a proglacial lake. Note that there can still be ice present underneath the lake [from Mertes et al., 2017].*

Proglacial lakes form at the termini of glaciers as supraglacial lakes merge and become dammed by a continuous moraine loop around the glacier terminus. They have the potential to significantly accelerate glacier mass loss [Benn et al., 2012; King et al., 2019]. This acceleration can occur through a reduction in the effective pressure (overburden pressure minus water pressure) due to high basal water pressures at the glacier-bed interface (eq. 1). The reduction leads to an increase in velocity through a decrease in basal friction. Consequently, the glacier terminus flows in the proglacial lake, with low resistance [Fowler & Ng, 2021].

$$N = P_i - P_w = \rho g H - P_w \quad [1]$$

Dynamic thinning is a result of the acceleration in flow velocity and ice discharge into the lake, leading to the thinning of the terminus [Pronk et al., 2021; Sato et al., 2022; Tsutaki et al., 2019]. As the glacier reaches the ice flotation level through thinning ($P_i = P_w$), the glacier terminus becomes subjected to buoyancy-induced calving. As ice flow heavily depends on the thickness of the glacier (H), thinning above the proglacial lake, combined with calving processes, will eventually lead to a retreat of the glacier terminus (eq. 2 and 3) [Pronk et al., 2021]. Another factor controlling ice flow velocities is the glacier surface slope ($sin\ \alpha$) as an increase in slope enhances the flow velocity.

$$\tau_d = \rho g H \ \sin\alpha \quad [2]$$

$$v = A\tau^n \quad [3]$$

The decreasing ice thickness through thinning results in a decrease of the driving stress (τ_d), which, according to Glen's flow law (eq. 3), reduces the flow velocity of a glacier (**fig. 3**). The proglacial lakes expand upwards if the glacier retreats, its initial position often remaining near the terminal moraine [Komori, 2008; Song et al., 2016], and can rapidly grow in area and volume [Kirkbride & Warren, 1999]. The expansion mechanisms for proglacial lakes in contact with a glacier, are the same as the expansion mechanisms for supraglacial lakes mentioned above (i.e. thermal notching, subaerial melt and calving) [Gardelle et al., 2011]. Although proglacial lakes mainly expand through calving [Fowler & Ng, 2021].

Subaqueous melt however plays a more important role in proglacial lakes compared to supraglacial lakes due to the greater depth of the lakes, resulting in more effective thermal undercutting [Truffer & Motyka, 2016].

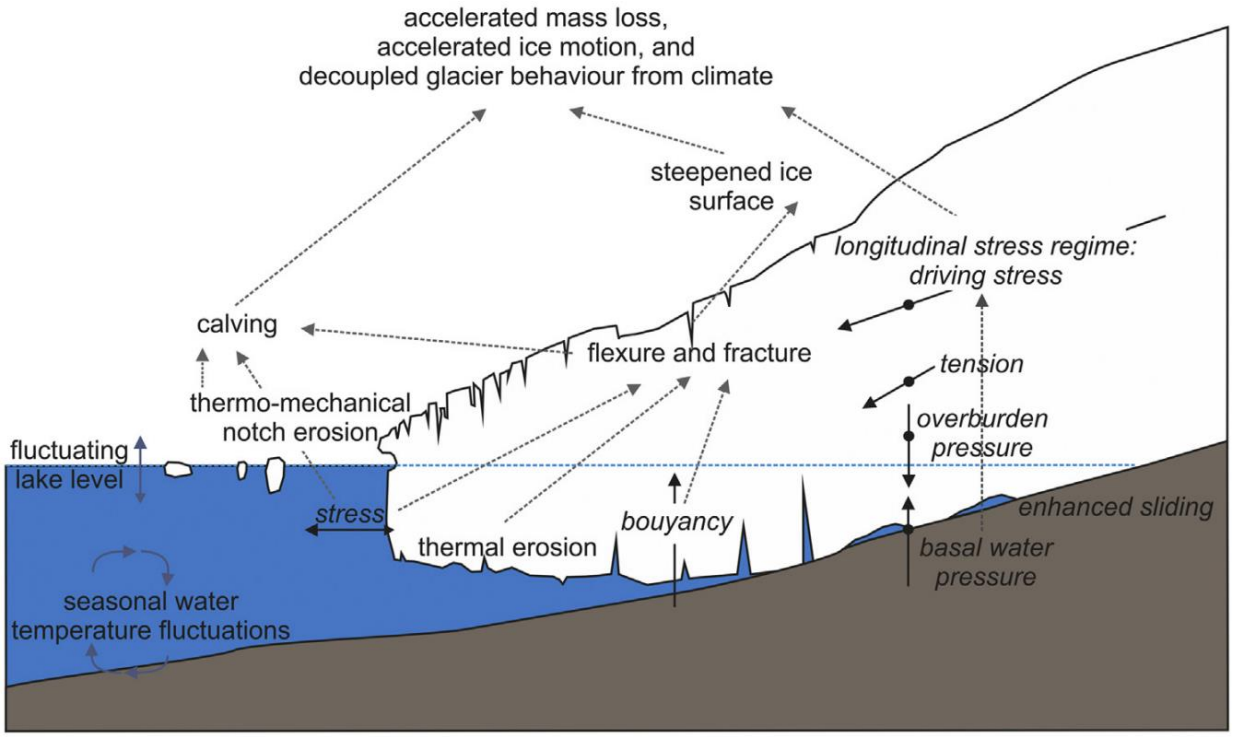

Fig. 3. *Schematic overview of the factors controlling glacier dynamics at the lake-glacier boundary. Processes are shown in black with grey dashed lines to highlight their interactions. Forces are shown in italic, with black arrows highlighting the direction of the force. The solid grey arrows indicate fluctuations mainly influenced by external forces (e.g. seasonal variations) [from Carrivick & Tweed, 2013].*

Calving is the main processes for the removal of large ice masses at the terminus for lake-terminating glaciers and occurs through episodic events varying over a wide range of temporal and spatial scales. The main processes responsible for calving are the growth of crevasses through tensile stresses or exploitation of weak spots in the ice, and hydrofracturing. Other important calving-inducing processes include buoyant forces, causing the terminus to float in the lake (through dynamic thinning) and the removal of ice at the base of the glacier terminus through subaqueous melt and thermal notching [Benn et al., 2012]. As a glacier calves, the resistive stresses on the ice reduce, resulting in a positive feedback where the ice flow increases, which promotes crevasses formation and increases calving [Nick et al., 2013]. Furthermore, the high thermal conductivity for water, allows for heat conduction through the lake which is often obtained from solar radiation. When the warmer water comes in contact with ice through water currents, driven by wind and temperature differences, it transfers part of the heat to the ice, resulting in localized ice melt and thinning. These processes lead to the formation of cavities and ice overhangings, or ice cliffs, and its instability might promote calving (**fig. 4**) [Fowler & Ng, 2021; Motyka et al., 2003; Sakai et al., 2009; Truffer & Motyka, 2016]. In equilibrium, the calving rate, c, is equal to the velocity at the terminus, u_f. If a disturbance changes these rates, it can result in a glacier retreating or advancing ($\frac{dL}{dt}$) (eq. 4). However, studies have not yet succeeded to establish a physical calving relation due to the limited understanding of related physical processes [Benn et al., 2007; Fowler & Ng, 2021]. Many lake-terminating glaciers show a retreat of their terminus, implying that the calving rate exceeds the glacier flow velocity.

$$\frac{dL}{dt} = u_f - c \qquad [4]$$

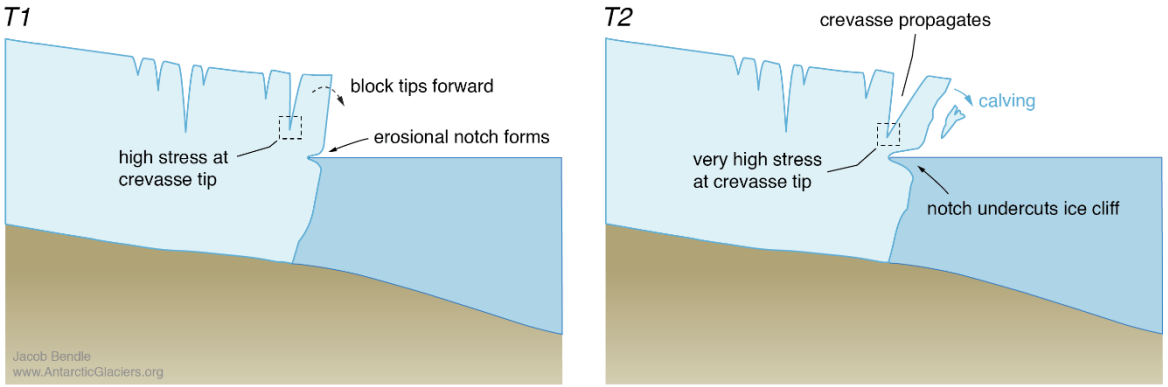

Fig. 4. *Schematic representation showing the effect of thermal undercutting and crevasse propagation due to hydrofracturing or changing stress regimes on calving. Note how the erosional notch is formed due to thermal notching [from: https://www.antarcticglaciers.org/glacier-processes/glacial-lakes/calving-of-freshwater-glaciers/].*

Multiple studies have shown that lake-terminating glaciers show higher mass losses than land-terminating glaciers, attributed to the processes described above. Lake-terminating glaciers account for 10-15% of the total glacier area in HMA, but were responsible for up to 32% of the observed mass loss between 2000 and 2015 [King et al., 2019]. Pronk et al. (2021) observed more than a doubling of glacier flow velocity between lake- and land-terminating glaciers (18.83 m yr^{-1} and 8.24 m yr^{-1}, respectively). From 2000 to 2020 proglacial lakes have increased by 47% in number, and also significantly in area and volume (33% and 42%, respectively) throughout the Himalayas. This increase has resulted in an even larger glacier mass loss in the last two decades [Zhang et al., 2015; Zhang et al., 2023].

The number of proglacial lakes in HMA is expected to increase even further. As reported by Furian et al. (2021) and Farinotti et al. (2019*a*) these lakes will differ from the existing lakes as they are expected to form in bedrock overdeepenings rather than behind terminal moraines. Overdeepenings form as glaciers erode the bedrock. When a glacier retreats, these depressions can store massive amounts of water and can become proglacial lakes. Although small overdeepenings are expected to mainly store sediments [Otto et al., 2021], there are still over 25.000 overdeepenings with areas larger than 10^4 m^2 in HMA with a potential to store large amounts of water, thereby also increasing the risk of GLOFs [Furian et al., 2021].

3. Study area

This study focuses on a selection of glaciers in the eastern Himalayan mountain range, located on the border between Bhutan and China. From west to east, these glacier are named G528, Bechung, Raphsthreng, Thorthormi and Lugge glacier (**fig. 5**). This glacier system is located at an elevation between 4400 and 7200 m a.sl. and extends southwards into the Bhutanese Lunana region (28°7’ N, 90°14’ E).

Debris-covered glaciers are common in this region, where the glaciers are confined to steep valleys with high rock avalanche activity [Bolch et al., 2012; Scherler et al., 2011]. Proglacial lakes are located in front of several glacier termini, varying in size. Supraglacial lakes have also be identified on several glaciers. Studies conducted by Bajracharya et al. (2014), Tsutaki et al. (2019) and Sato et al. (2022) mapped the flow velocities and thinning rates of the lake-terminating Thorthormi and Lugge glaciers located in the same study area. These studies have demonstrated the long-term mass loss of these Bhutanese glaciers over recent decades.

Bhutan is strongly influenced by the Indian and the south-east Asian summer monsoons, where most precipitation occurs from June to September [Böhner, 2006]. During this period, the monsoons supply up to 80% of the annual precipitation to the eastern Himalayas [Bookhagen & Burbank, 2010]. The Himalayas act as an orographic barrier and deplete most of the air of precipitation, resulting in dry winds down on the Tibetan Plateau. As a result, a general decrease in moisture northwards is observed [Bolch et al., 2012]. Since the monsoons provide both precipitation and high temperatures, glacier accumulation and ablation occur simultaneously in the Himalayas [Ageta & Higuchi, 1984]. This makes Bhutanese glaciers especially sensitive for climate change, as it might alter temperature and precipitation patterns during the monsoon season [IPCC, 2021; Sakai & Fujita, 2017].

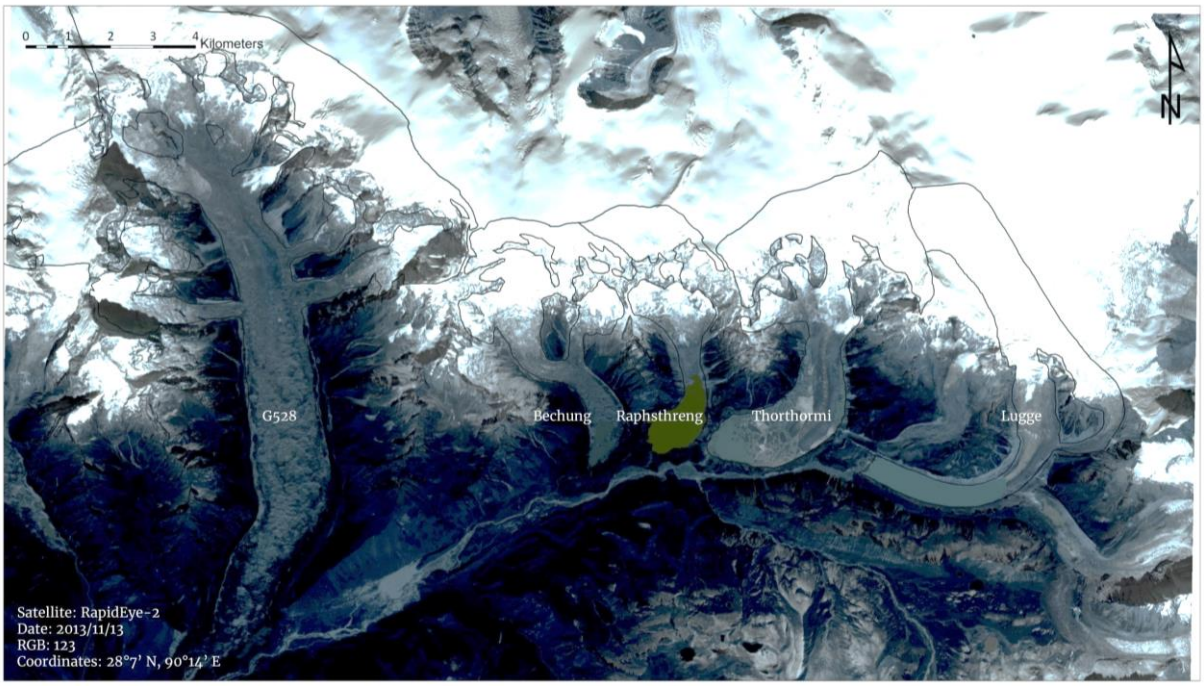

Fig. 5. *RapidEye image of the Lunana region in November 2013, showing the outlines from the selected glaciers.*

4. Data and methods

4.1 Data

Remote sensing has significantly increased our understanding of the cryosphere by providing high quality imagery on a broad scale of applications with varying spatiotemporal scales [Tedesco, 2015; Van Wyk de Vries & Wickert, 2021] This research incorporates satellite images from three different sources: Landsat, RapidEye and PlanetScope.

Landsat 4-5 TM and Landsat 8-9 OLI/TIRS data was extracted from https://earthexplorer.usgs.gov/, with a resolution of 30 m. The Landsat satellites carry bands ranging from the visible spectrum to the near-infrared (NIR) and shortwave infrared (SWIR). Landsat 5 TM was specifically chosen due to the Scan Line Corrector (SLC) failure in 2003 that affected Landsat 7 ETM+. The SLC led to gaps in the data, making interpolation or gap-filling methods necessary, resulting in unnecessary uncertainties. Landsat 8-9 was used to derive glacier velocities in 2013-2014. RapidEye and PlanetScope are two satellite constellations owned by Planet Labs. They are known for their high spatial resolution (6.5 and 3 meters, respectively) at high frequency and are therefore ideal for lake detection and feature tracking, for which high spatiotemporal resolution is often required. These satellites carry bands ranging from the visible spectrum to the NIR. The RapidEye and PlanetScope images were obtained from https://www.planet.com/explorer/.

For the lake detection, a single satellite image was collected for (almost) every year between 2003 and 2023. To minimize cloud and snow cover, and to avoid the freezing of the lakes later in the season, the images were collected between September and December [Tsutaki et al., 2019]. This narrow time window also leads to low seasonal differences which might impact the results. Prior to the selection, all images were visually inspected to check for the absence of snow around the lake perimeter, minimal cloud and snow cover, and minimal shadowing over the glaciers that might distort the results. An overview of the selected images for lake detection is given in **tab. A1**. To derive glacier velocities, specific years are selected instead of time series as feature tracking software is sensitive for large jumps in time and processing twenty years of imagery is highly time-consuming [Van Wyk de Vries & Wickert, 2021]. The specific years are selected based on the spatiotemporal evolution of glacial lakes, including periods characterized by rapid retreat or changes in lake development. High resolution Planet imagery is most optimal, but Landsat 4-5 and 8-9 scenes were also applied to account for earlier years and to evaluate the use of images with lower resolution (**tab. A2**).

The Randolph Glacier Inventory (RGI v7), released in 2023, is a global database representing the glacier outlines in 2000 [RGI Consortium, 2023]. As a result, glaciers with relatively high flow velocities and mass loss might differ significantly from these outlines. Besides providing glacier extents, the RGI also offers data regarding elevation, area and slope, among others (**tab. 1**).

Glacier name	*RGI v7 ID*	*Type of lake*	*Area (km^2)*	*Slope (°)*
*G528**	RGI2000-v7.0-G-15-09528	Supraglacial	48.8	22.7
Bechung	RGI2000-v7.0-G-15-09530	Proglacial	8.41	28.8
Raphsthreng	RGI2000-v7.0-G-15-09531	Proglacial	4.49	24.8
Thorthormi	RGI2000-v7.0-G-15-09532	Proglacial	13.2	21.2
Lugge	RGI2000-v7.0-G-15-09534	Proglacial	10.3	15.8

Tab. 1. *Table providing information of the selected glaciers in the study area. Note that the provided data stems from 2000 [RGI Consortium, 2023]. *G528 is the name of the westernmost glacier referred to in this study since it does not have an official name.*

NSIDC provided changes in ice thickness from 1975 to 2017 with a resolution of 30 m [Maurer et al., 2019]. From 2017 to 2022, the DEMs and thickness changes were constructed and provided by dr. Brun from the University of Grenoble Alpes using Pléiades imagery, with a resolution of 4 m. These datasets will be used to calculate the glacier thinning rates.

4.2 Methods

4.2.1 Pre-processing

The extracted satellite imagery required preprocessing to make it usable. Landsat images are initially available as individual bands, and had to be converted into composite images (RGB). Since the study area was fully covered in a single image, mosaicing was not required. In addition, the images were already atmospherically corrected and georeferenced. The RapidEye scenes, similar to Landsat, are provided as individual bands, requiring a conversion into composite images. Occasionally, multiple images covered the study area which required mosaicing. The images had undergone atmospheric correction; however, the process of georeferencing was repeated due to its poor quality. PlanetScope images can be acquired as composite images, but consist of multiple scenes. Mosaicing of the individual scenes was therefore necessary. PlanetScope images can be downloaded with usable atmospheric correction and georeferencing, reducing the need for these processes. It is important to note that besides the poor georeferencing, RapidEye images can vary significantly in viewing angle compared to PlanetScope and Landsat imagery. This can lead to stretching or compression of glacial features, and can thus lead to erroneous results and interpretations. With this in mind, the most optimal RapidEye imagery was selected and corrected to enhance its accuracy and utility. For deriving glacier flow

velocities, RapidEye imagery was excluded from the selection since feature tracking tools require high georeferencing standards. Instead, Landsat 8-9 images were used.

The glacier outlines, provided by the RGI, are used to clip the selected glaciers from the images, effectively excluding background noise like shadows and mountain snow cover. However, the RGI does not include outlines of the glacier lakes. To map the development of glacial lakes, the extent was expanded to include the lakes. When deriving the flow velocities, the extents were corrected to only cover the glaciated area, excluding bedrock and water, preventing potential misinterpretations by the software.

The changes in ice thickness between 1975 and 2017 contained some gaps in the data. These gaps were interpolated as accurately as possible and visually inspected to prevent large deviations in the interpolated dataset which might lead to erroneous results.

4.2.2 Mapping spatiotemporal lake evolution

The spatiotemporal evolution of glacial lakes was studied using 19 satellite images between 2003 and 2023 (**tab. A1**). Between 2003 and 2008, 30 m resolution Landsat 4-5 images were applied to the glaciers. Following this, RapidEye (2009-2015) and Planet images (2016-2023) were used with 6.5 m and 3 m resolution, respectively. The NDWI was computed following Watson et al. (2018) and Lesi et al. (2022) by measuring the difference in reflectance between the green and NIR wavelengths (eq. 5). Since the difference is higher for water than for snow and ice, glacial lakes can be identified. An empirical threshold with the most optimal signal-to-noise ratio was applied to separate the water pixels from the non-water pixels. This threshold increases with increasing resolution as less mixed pixels (containing land or ice) occur, which mainly affects low resolution imagery [Ji et al., 2009; Nagy & Andreassen, 2019]. This resulted in varying thresholds for Landsat, RapidEye and PlanetScope imagery of 0.11-0.13, 0.30-0.34 and 0.34-0.38, respectively (**tab. A1**). The variability in thresholds for the same satellites can be attributed to several processes, including atmospheric conditions, seasonal variations or water quality.

$$NDWI = \frac{Green - NIR}{Green + NIR} \quad [5]$$

A pixel is classified as a lake if the NDWI exceeds the set threshold and the pixel is located within the glacier extent. Furthermore, a slope map, extracted from the 2017 Pléiades DEM, was applied on the G528 glacier to filter out noise as supraglacial lakes only form on shallow slopes (< 3°) [Gardelle et al., 2011]. Glacial lakes were mapped by polygonising the remaining pixels which were visually inspected and corrected before calculating the statistics. Visually, the mapping of the lakes proved to be relatively accurate. Therefore, the empirical minimal mapping unit (MMU) was set to relatively low values of $\frac{2}{3}$ (900 m^2), 4 (169 m^2) and 16 (144 m^2) pixels for Landsat, RapidEye and PlanetScope respectively. For the Thorthormi glacier, the whole lake was manually corrected for due to the continuous presence of ice and debris in the lake which hampered the automatic mapping.

4.2.3 Deriving glacier flow velocity

4.2.3.1 Feature tracking

Feature tracking is an important method to better understand glacier behavior by highlighting ice displacement in glaciated regions through remote sensing imagery. This technique makes it possible to observe variations of glacier velocities over both space and time. Feature tracking can therefore be used to assess changes in ice flow dynamics related to climate change or glacial lakes, among others [Ahn & Howat, 2011; Heid & Kääb, 2012; Kääb, 2005].

Feature tracking makes use of co-registered images, in which the properties of two images are compared to derive the location of optimal fit in an image with respect to the other. This is done by dividing individual images in a grid consisting of smaller images called 'chips'. A correlation coefficient is calculated for each chip in the first image (X1). Next, X1 is compared to a surrounding area within the second image (X2), where the best fit is characterized by a high correlation coefficient. If the chip is recognized at the same position in X2, with respect to X1, no displacement has occurred. If, however, the chip is matched at a different location in X2 with respect to X1, displacement has occurred. Consequently, the pixel displacement between both chips is calculated [Heid & Kääb, 2012; Luckman et al., 2007; Van Wyk de Vries & Wickert, 2021].

4.2.3.2 Glacier Image Velocimetry

This study used the newly developed feature tracking tool Glacier Image Velocimetry (GIV) by Van Wyk de Vries (2021*a*). GIV is an open-source toolbox developed to easily calculate glacier flow velocities. Extensive research has shown that it can output high spatiotemporal resolution surface flow velocity products of all types of glaciers [Van Wyk de Vries & Wickert, 2021]. While it is written in MATLAB, users can exploit GIV through MATLAB functions or a standalone desktop app [Van Wyk de Vries, 2021*a*]. This study makes use of the latter.

To successfully run GIV, the collected satellite images were stored in a single folder and named accordingly to YYYYMMDD (e.g. 20201030). In this folder, a *save_image*, *stable* and *mask* file were also present. The *save_image* is the best satellite image of the time series which is used in the plotting stage. The *stable* image is a mask of the bedrock which is left out in the calculation of the velocity. It is important not to mask water since this can lead to distortions in the outputs. The *mask* file is the mask of the glaciated areas that the feature tracking tool will be applied to [Van Wyk de Vries, 2021*b*].

Typically, images are run sequentially. However, GIV includes a temporal oversampling factor (TOF), which also calculates glacier velocities based on non-consecutive images, resulting in a substantially increased final dataset. In this study, the TOF is set to the highest possible value, determined by $n - 1$, where n is the total number of images (6 images would have a maximum TOF of 5). In addition, the resolution of the velocity maps were tuned to the highest possible resolution, resulting in 12 m for PlanetScope and 120 m for Landsat imagery. Finally a multi-pass method was applied to the imagery in which displacements are calculated more accurately by using smaller windows in subsequent passes, leading to high spatial resolution and fine details [Van Wyk de Vries, 2021*b*; Van Wyk de Vries & Wickert, 2021].

Constructing flow velocities on glaciers is challenging due to dynamic glacier changes over time. Factors such as the opening and closing of crevasses, snow cover and melting processes all contribute to this. In addition, processing satellite images need to adress factors such as variations in viewing angle, shadows and cloud cover [Kääb et al., 2016]. GIV incorporates various noise-reducing filters and filters designed to highlight glacial features such as crevasses or debris, which can be set prior to running the tracking tool for enhanced performance. For this study, an orientation filter was applied which enhanced the magnitude of glacial features, making them easier to track. Also a spatiotemporal smoothening was applied to the velocity maps to fill gaps in the data. Finally, to correct for erroneous flow velocities due to mismatches in the software, outliers were automatically removed by comparing the mean and standard deviation values of each grid cell to their neighboring cells [Van Wyk de Vries & Wickert, 2021].

4.2.3.3 Model run and output data

When running GIV, the chip is matched in the frequency domain through a 2D correlation. The chip and the search area are transformed into the frequency domain through a FFT (Fast Fourier Transform).

Here, the chip is compared to different parts of the search area looking for similarities by multiplying them together. When completed, the results are converted back to the spatial domain using an inverse FFT. This process is repeated for each chip in the original image. By converting the image to the frequency domain, it is computational efficient as it calculates the correlation across the whole image at once [Van Wyk de Vries & Wickert, 2021]. The outputs are saved in folders, containing georeferenced files of the median and mean flow velocity, flow direction, and the x- and y-components of the velocity, among others. In this study, the median flow velocity files were used since median values are not affected by exceptionally high or low values.

4.2.4 Thinning rates and glacier mass balance

The thinning rates and associated mass loss are calculated between 1975 and 2022. Between 1975 and 2017, the thinning rates were extracted from Maurer et al. (2019). This dataset contains the annual mean ice thickness change from 1975 to 2000, and from 2000 to 2017. From 2017 to 2022, the thinning rates were calculated using Pléiades DEMs through DEM differencing. In this process, one DEM is extracted from the other, yielding the change in ice thickness per pixel between 2017 and 2022. By dividing this change over the total years, the mean ice thickness change or thinning rate (Δh) per year was obtained. For each glacier, the statistics related to the thinning rate were calculated, including the mean, minimum and maximum.

The mass balance over the whole glacier (b) was calculated, where the mean thinning rate is multiplied by the density ratio of ice (ρ_i = 850 kg m^{-3}; [Huss, 2013]) and water (ρ_w = 1000 kg m^{-3}). The unit is in m w.e./yr (eq. 6). To determine the total mass which had been gained or lost, the mean thinning rate was multiplied by the total glaciated area (A). The total mass change (ΔM) could then be derived by multiplying the volume by the ice density (eq. 7) and is given in Mt yr^{-1} [Shean et al., 2020].

$$b = \Delta h \frac{\rho_i}{\rho_w} \quad [6]$$

$$\Delta M = \Delta h A \rho_i = \Delta V \rho_i \quad [7]$$

4.2.5 Post-processing

During the post-processing stage, the output data from the methods were processed and converted into usable graphs using Python. Trendlines were fitted to the lake evolution data, while the Pleiades DEM was divided into 50 m elevation bands to analyze the temporal changes in area and number of supraglacial lakes on the G528 glacier. The surface flow velocities resulting from GIV were extracted along the flowline of the glacier, which is characterized by the highest flow velocities due to increased deformation and minimal lateral drag. Deriving the velocities from the flowline resulted in a more straightforward assessment of variations in velocity over time. The flowlines were provided by Van Huizen (2024). In Python, the velocities were buffered within a 200 m width from the flowline and averaged at 50 m intervals along the flowline to account for local uncertainties. In addition to the flow velocities, the thinning rates were extracted from the flowline within a 100 m width from the flowline, due to higher resolutions, and averaged at 50 m intervals. Since the elevation and slope also significantly control the glacier flow velocity and thinning rate, the elevation profile was extracted from the flowline using the Pléiades DEM from 2017, applying the same parameters as the thinning rate along the flowline. The position of the glacier front (**tab. A3**) was determined to filter out erroneous velocity and thinning rate data displayed in the graphs. This was done by measuring the distance along the flowline to the glacier front using satellites images.

Finally, during the NDWI process pixels classified as lakes might include mixed pixels, i.e. representing a mix between lake and land. This uncertainty is especially high in low resolution imagery [Qayyum et al., 2020]. To calculate the uncertainty by these mixed pixels, the equations of Hanshaw & Bookhagen

(2014) and Lesi et al. (2022) were applied. The number of pixels around the lake were computed by dividing the perimeter (P) by the grid size (G) and multiplying it by 1σ. The 1σ (standard deviation) indicates that approximately 69% (0.6872) of the pixels are susceptible to error, as 69% of the data falls within one standard deviation of the mean, following a Gaussian distribution. Assuming that the uncertainty comprises half a pixel rather than a full pixel, the number is multiplied by half of the area of a pixel (eq. 8). The relative error (D) was computed by dividing the number of edge pixels by the area (A) (eq. 9) [Hanshaw & Bookhagen, 2014; Lesi et al., 2022].

$$Error(1\sigma) = \frac{P}{G} \cdot 0.6872 \cdot \frac{G^2}{2} \quad [8]$$

$$D = \frac{Error(1\sigma)}{A} \cdot 100\% \quad [9]$$

5. Results

5.1 Spatiotemporal evolution of lakes

This section covers the spatiotemporal evolution of the glacial lakes between 2003 and 2023. The results are shown in **figure 6**, where the black areas indicate the glacial lakes. This figure shows that the proglacial lakes have grown over time and mainly expanded upwards. **Figure 7** shows how the proglacial lake area expanded over time, supported by **table 2** showing the mean annual expansion rate of the lakes.

Between 2003 and 2023, no proglacial lake has formed in front of the G528 glacier. However, the glacier is spotted with supraglacial lakes, increasing in area over time as smaller lakes merged together. The lakes in front of the Bechung, Raphsthreng and Lugge show a steady, linear expansion over time (**fig. 7**). The Bechung glacier was characterized by multiple smaller lakes in 2003, which merged over several years to form one large lake in 2010, which expanded with 22,591 m^2/yr. In recent years, many supraglacial lakes formed and disappeared on elevations above its main lake. The Raphsthreng glacial lake showed a minimal increase in lake area (8,516 m^2/yr) with some moments of glacier advances which temporarily decreased the lake area. On this glacier some supraglacial lakes were be identified although in small numbers. The expansion of the Lugge glacial lake has also been gradual over the last twenty years, but shows the largest expansion rate of the three (28,421 m^2/yr).

The most significant changes can be observed at the Thorthormi. Between 2003 and 2010, glacial lakes have extended on the sides of the glacier, where smaller lakes and ponds spotted the glacier surface, increasing in size and coalescing over the years. Between 2010 and 2012, the glacier detached from the terminal moraine. From 2012 to 2022 the glacier retreated rapidly. From 2015, large cracks in the side of the glacier tongue started to form, and from 2018 the cracks propagated all the way into the interior of the glacier tongue. In 2021, the Thorthormi terminus merely existed of a floating, disintegrating ice tongue. The whole tongue in the glacial lake disappeared in 2022 and the glacier terminus retreated on higher elevations. In **figure 7**, the Thorthormi glacial lake shows an exponential increase over time, which comes to a halt in 2022 and 2023. The arrow indicates the moment of detachment from the terminal moraine. The average rate of expansion is significantly higher for the Thorthormi compared to the other glaciers, especially from 2012 to 2022 as the expansion rate almost doubled to 225,333 m^2/yr compared to 2003-2011. Since the lakes mainly expanded upwards, as the initial position remained near the terminal moraine, the annual lake expansion rate (**table A4.1-4.4**) can also be regarded as the annual reduction in glacier area.

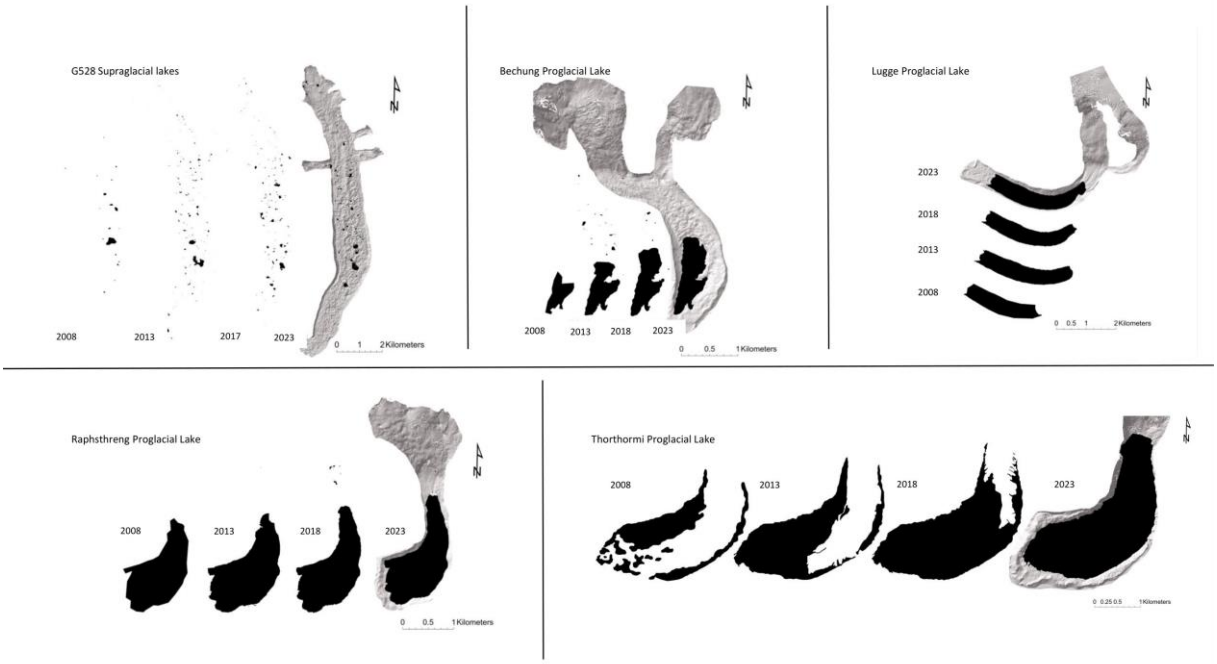

Fig. 6. *The development of glacial lakes in the Lunana region from 2008 to 2023. The black regions represents the lake area. Each of the lakes in 2023 is underlain by a Pléiades hillshade of each glacier from 2022.*

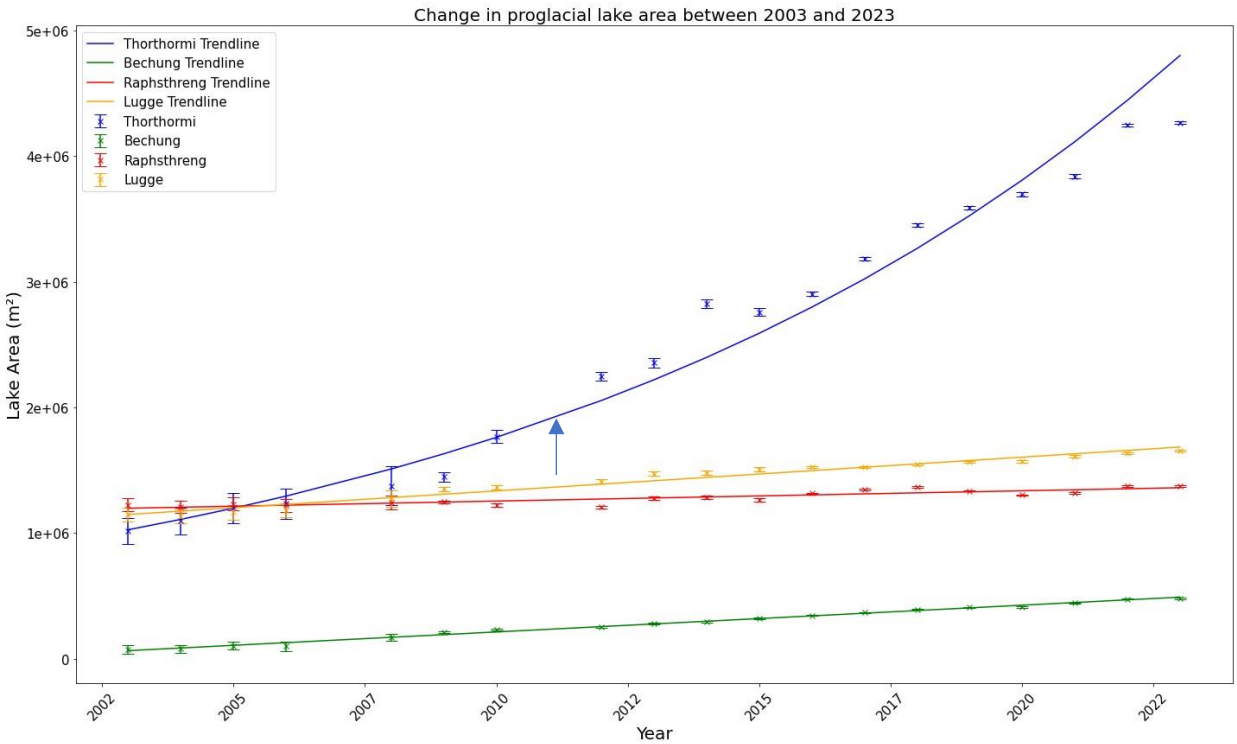

Fig. 7. *Graph showing the expansion of the proglacial lakes in m^2 between 2003 and 2023, with the error bars in place. The blue arrow indicates the transition of the Thorthormi from land-terminating to lake-terminating in 2011. The lake areas per year are highlighted in* **table A4.1-A4.4**.

	Thorthormi	*Bechung*	*Raphsthreng*	*Lugge*
Mean expansion rate (2003-2023) (m^2/yr)	180,541	22,591	8,516	28,421
Mean expansion rate (2003-2011) (m^2/yr)	125,521	-	-	-
Mean expansion rate (2012-2022) (m^2/yr)	225,333	-	-	-

Tab. 2. *Table showing the mean expansion rate for each glacier in m^2/yr. For the Thorthormi, the mean expansion rate for 2003 to 2011 and 2012 to 2022 is shown as well, to highlight the land- and lake-terminating phase of the glacier.*

5.2 Surface flow velocity of glaciers

This section gives an overview of the changes in surface flow velocity along the flowline over five periods (i.e. 2006, 2013, 2017, 2020 and 2022) calculated with GIV. The velocity regime of each glacier will be compared to its corresponding elevation profile along the flowline. In the graphs, the 2006 and 2013 data are represented by Landsat data, whereas 2017, 2020 and 2022 are represented by PlanetScope imagery, allowing for the comparison between both satellite systems. The glacier velocities stop at the glacier front, where the glacier makes contact with the proglacial lake, to filter out erroneous data. The glacier front was determined by calculating the distance at which the flowline reached the glacier front for each defined period. The figures presented in this section consist of a graph of the surface flow velocity along the flowline; and an elevation profile of the corresponding glacier along the flowline projected above. The figure projected at the right shows the NDWI-derived lake outlines for each year with the flowline projected on top, underlain with a PlanetScope image from 2023.

The G528 glacier in **figure 8** shows the highest velocities, ranging from 100 to over 200 m/yr on the steepest part of the glacier. The largest part of the glacier however, is characterized by relatively low velocities, ranging from almost 0 to 40 m/yr, corresponding to the shallow slope of around 1.14°. The glacier has experienced no retreat between 2003 and 2023. The flow velocities are highest in 2006 and 2013. The velocities in 2017 are lower but are slightly increasing again over 2020 and 2022. No crevasses are observed on the shallow parts of the glacier. On the steeper parts of the glacier, transverse and marginal crevasses are observed.

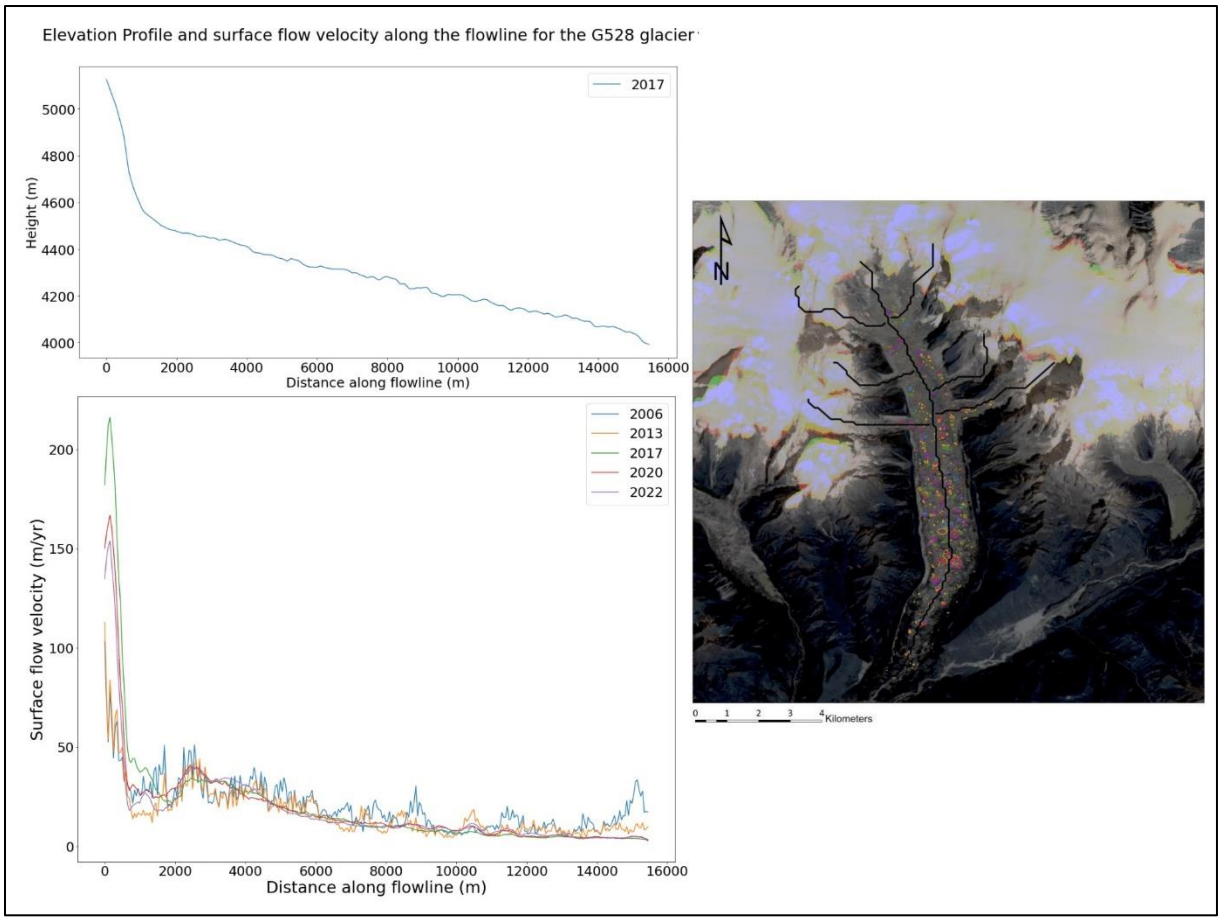

Fig. 8. *The graphs on the left show the surface flow velocity (lower) and the elevation profile (upper) along the flowline of the G528 glacier, averaged at 50 m intervals. The extent of the flowline is illustrated in the image on the right. The colored lake outlines in the image, correspond to the colors of the years in the velocity graph.*

The Bechung glacier is characterized by high velocities of over 200 m/yr on the steepest parts of the glacier between 1000 and 2000 m along the flowline (**fig. 9**). In 2006 and 2013 the velocities reached a maximum of 50 and 80 m/yr, respectively. In 2017 and 2020, the velocities were much higher at this point, above 200 m/yr, although lower in 2020 compared to 2017. In 2022, the velocity dropped to around 180 m/yr. For all the years, a rapid decrease in velocity marks the shallow part of the glacier, where the velocities reach values of up to 25 m/yr. This is also the region where the glacial lake expands upwards over time, marked by a retreat of the glacier front. The outlines on the right image shows that the Bechung glacier is characterized by multiple supraglacial lakes.

The front of the terminus is characterized by transverse crevasses stretching partly along the front, and approximately 100 m along the flowline. On higher elevations, marginal and transverse crevasses can be identified. Furthermore, the Bechung lake is characterized by a low number of small icebergs of a few meters in diameter, with the largest up to 20 m. Most of the icebergs are accumulating directly underneath the glacier front.

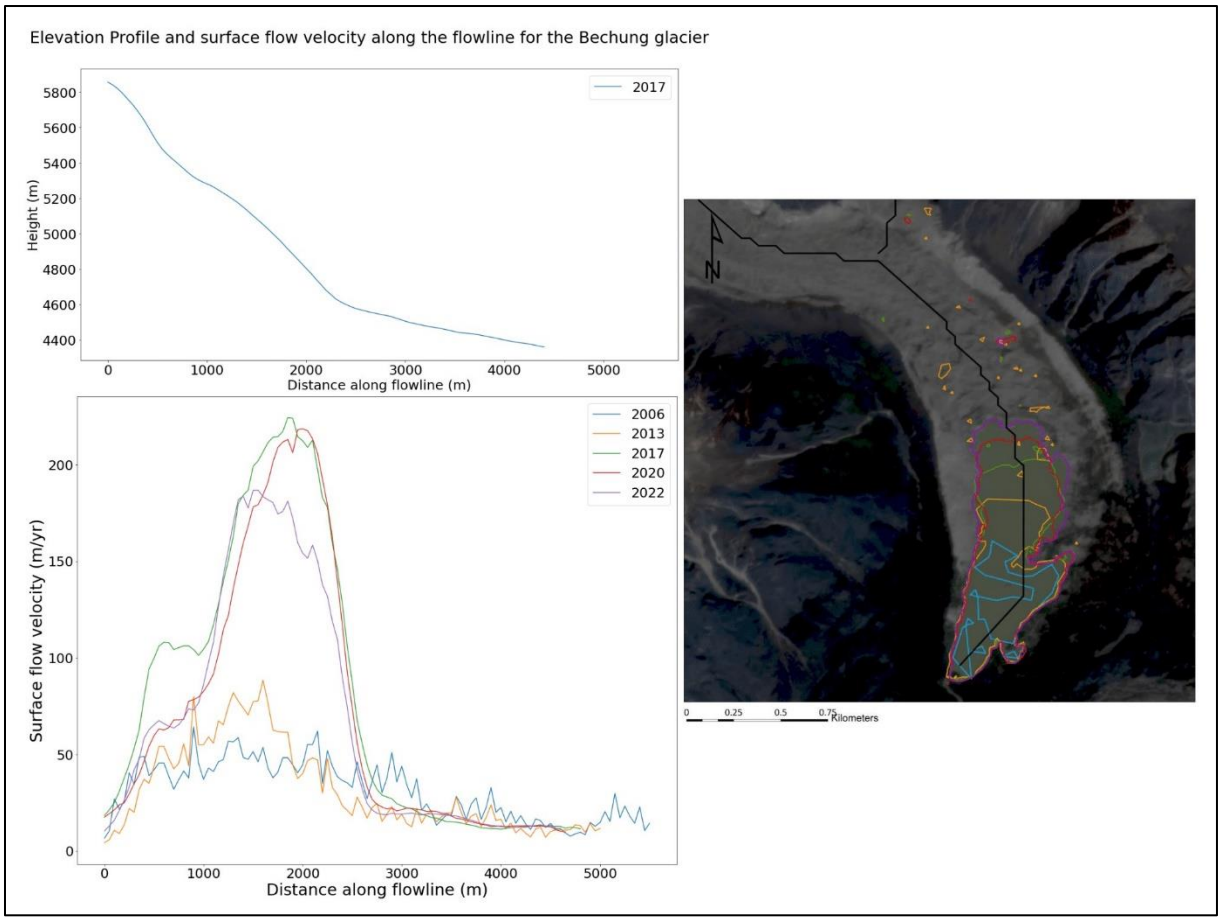

Fig. 9. *The graphs on the left show the surface flow velocity (lower) and the elevation profile (upper) along the flowline of the Bechung glacier, averaged at 50 m intervals. The extent of the flowline is illustrated in the image on the right. The colored lake outlines in the image, correspond to the colors of the years in the velocity graph.*

The Raphsthreng glacier shows relatively low surface flow velocities at the highest altitudes, although increasing downglacier (**fig. 10**). The region with the highest velocities is characterized by the steepest slope between 1000 and 1500 m along the flowline. The velocities in this region for 2006 and 2013 are relatively low with peaks up to 60 m/yr for both years approximately. From 2017 to 2022 this region shows much higher velocities, but shows a significant decrease from over 140 m/yr in 2017 to around 95 m/yr in 2022. On the lowest part of the glacier, with the smallest slope, the velocities show a sharp decrease. The maximum velocities in this region are 45 m/yr in 2017, decreasing in 2020 to around 20 m/yr. The lake outlines show that between 2017 and 2020, the glacier front advanced corresponding to a sudden decrease in velocity of 40 m/yr, which increased again in 2022.

As at the Bechung glacier, the front of the Raphsthreng glacier is characterized by transverse crevasses which stretch partly along its front, and approximately 100 m along the flowline. On higher elevations, marginal and transverse crevasses were also identified. Moreover, the Raphsthreng lake is characterized by a low number of small icebergs of a few meters in diameter, with the largest up to 15 m. Most of the icebergs are accumulating directly underneath the glacier front, and very few icebergs were observed far out on the lake.

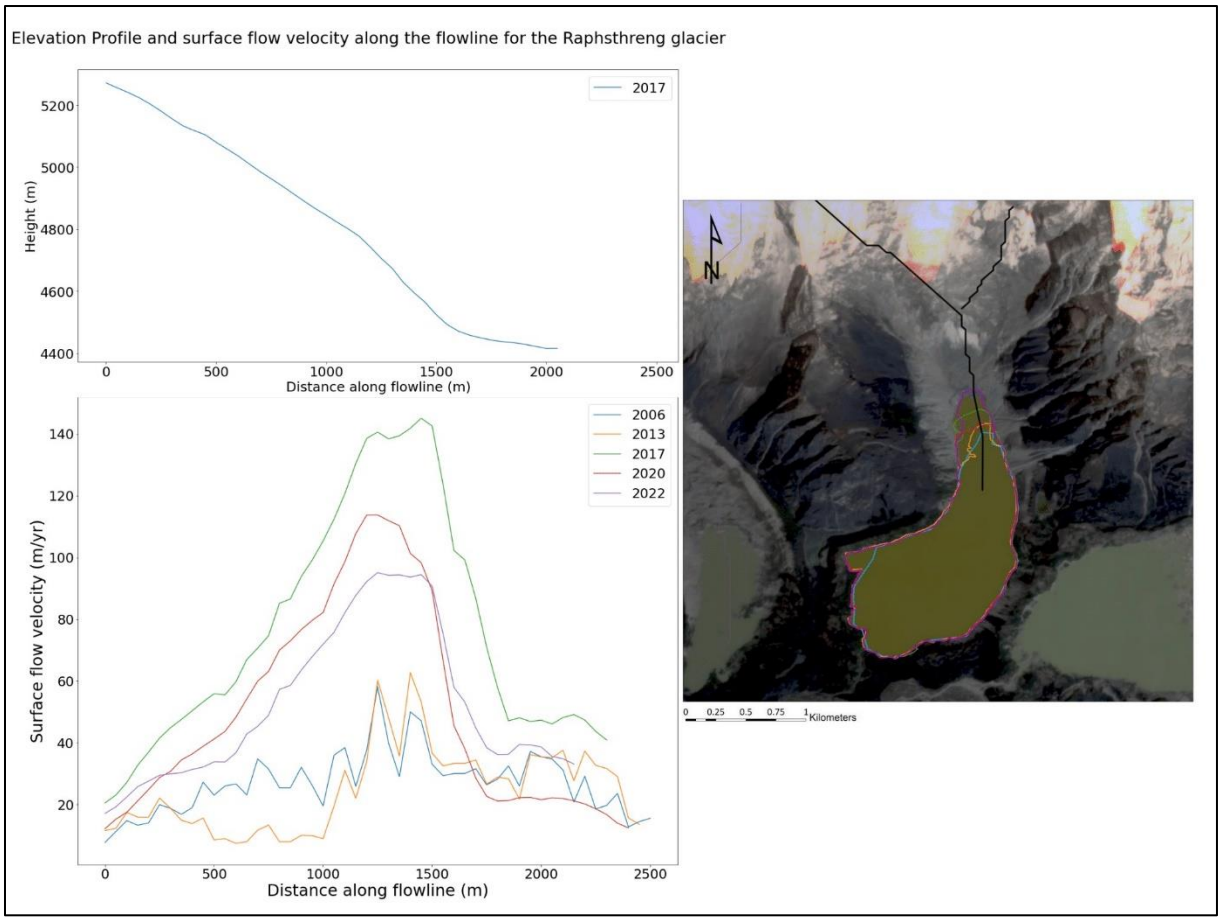

Fig. 10. *The graphs on the left show the surface flow velocity (lower) and the elevation profile (upper) along the flowline of the Raphsthreng glacier, averaged at 50 m intervals. The extent of the flowline is illustrated in the image on the right. The colored lake outlines in the image, correspond to the colors of the years in the velocity graph.*

The velocities of the Thorthormi glacier (**fig. 11)** show the opposite of the Bechung and Raphsthreng velocities. For 2006 and 2013, the Thorthormi showed relatively similar and constant velocities across the whole glacier, with the lowest velocities at the terminus and gradually increasing upslope (5 to 90 m/yr). For 2017 and 2020, the steepest part of the glacier is characterized by the lowest velocities of 40 and 20 m/yr, respectively. On the flat terminus, there is a sharp increase in flow velocity, reaching 260 and 230 m/yr, respectively. On the contrary, in 2022, the steepest part is characterized by higher velocities compared to 2017 and 2020, between 100 and 120 m/yr. The glacier front is located on the steep slope, characterized by velocities of approximately 120 m/yr.

The Thorthormi lake is characterized by an exponential increase in the area as is explained in section 5.1, which can also be observed in the lake outlines in **figure 11**. From 2022, the glacier front is characterized by transverse crevasses, extending for over 250 m inwards along the flowline. On higher elevations, marginal crevasses and transverse crevasses can be observed. The lake surface is scattered with icebergs, varying significantly in size from 1 m up to over 500 m in diameter.

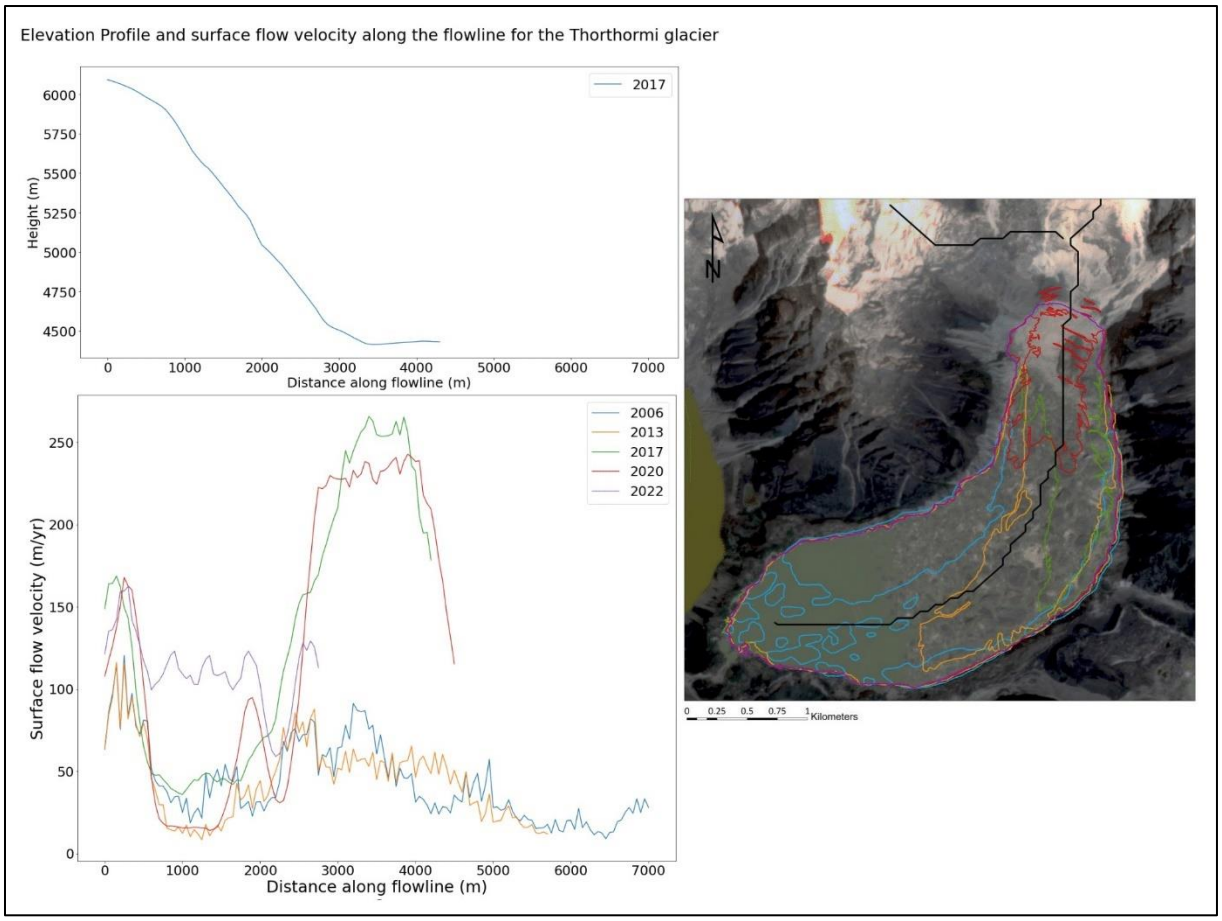

Fig. 11. *The graphs on the left show the surface flow velocity (lower) and the elevation profile (upper) along the flowline of the Thorthormi glacier, averaged at 50 m intervals. The extent of the flowline is illustrated in the image on the right. The colored lake outlines in the image, correspond to the colors of the years in the velocity graph.*

Finally, the Lugge glacier is also characterized by the highest surface flow velocities in the steepest regions of the glacier between 1000 and 2200 m along the flowline (**fig. 12**). On higher elevations the velocity is relatively low but increasing downslope. For 2006 and 2013, the velocities in this region lie between 75 and 125 m/yr, where for 2017 to 2022, the velocities are much higher. Furthermore, between 2017 and 2022, the velocities remained mainly constant at 200 m/yr. Just as at the Bechung and Raphsthreng glaciers, there is a clear decrease in velocity when the slope decreases. However, as the velocities of other glaciers decreased over time at the glacier front, the ice flow of the Lugge showed an acceleration towards the front in this period with velocities from 40 m/yr in 2017 and 2020 to 75 m/yr in 2022.

The whole front of the Lugge terminus is characterized by transverse crevasses, covering a large area, as a region of transverse crevasses extends to over 400 m inwards along the flowline. On higher elevations, transverse and marginal crevasses can be observed. The Lugge glacial lake shows a higher number of larger icebergs compared to the Bechung and Raphsthreng, often ranging from 1 to 40 m, although larger ones were sporadically observed up to 60 m in diameter. Moreover, the glacier front occasionally shows significant increases in iceberg discharge, leading to the formation of larger, tabular icebergs in its lake. Unfortunately, it is challenging to assign a specific temporal window for these increased discharges, since they were not consistently captured in every satellite image.

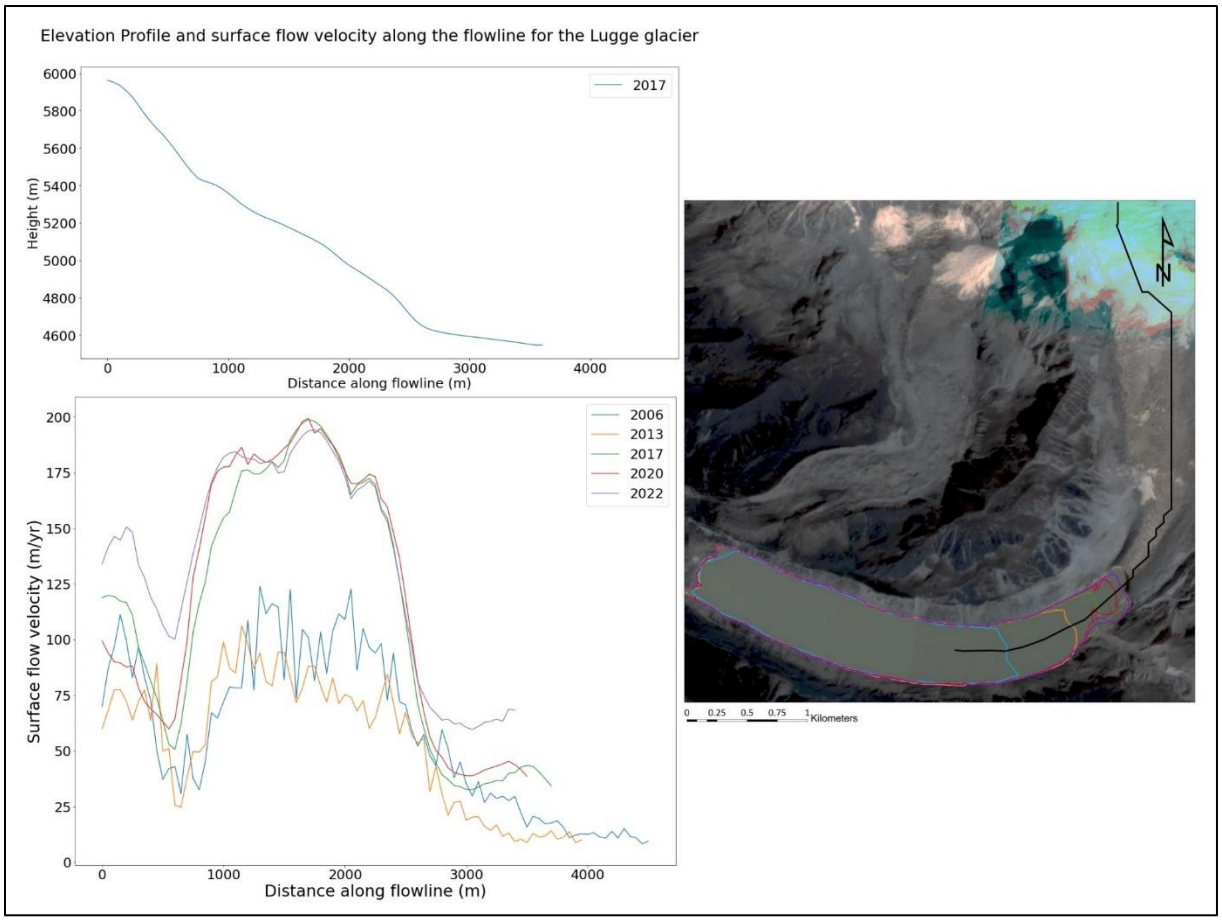

Fig. 12. *The graphs on the left show the surface flow velocity (lower) and the elevation profile (upper) along the flowline of the Lugge glacier, averaged at 50 m intervals. The extent of the flowline is illustrated in the image on the right. The colored lake outlines in the image, correspond to the colors of the years in the velocity graph.*

5.3 Thinning rates of glaciers

This section shows the thinning rates, or change in ice thickness, over three defined periods, namely 1975-2000, 2000-2017 and 2017-2022. The plots of each specific period stop at the glacier front of the final year of each specific period, to remove possible distorted values related to the presence of icebergs or fluctuations in the lake water level. **Figure 13** shows the graphs of the thinning rates per glacier. The map provides the spatial variation of the annual thinning rates between 2017 and 2022. Important to note is that the negative values presented in this section correspond to glacier thinning, and positive values to glacier thickening. An increase in thinning rate means an increase in glacier thinning (i.e. negative values becoming more negative), whereas a decrease in thinning rate means a decrease in glacier thinning (i.e. negative values becoming less negative). The mean annual thinning rate is calculated over the whole glacier, and not along the flowline, to derive the mass balance and mass loss for each glacier presented in **figure 14**.

The G528 glacier (**fig. 13a**) is characterized by an extremely fluctuating thinning rate, varying between an average of 2.5 to -2.5 m/yr between 2017-2022. Despite the large flux, the thinning has been increasing over years, with average rates of -0.43, -0.76 and -0.96 m/yr for 1975-2000, 2000-2017 and 2017-2022, respectively. On the middle part of the glacier, glacier thinning is highest compared to the upstream and downstream part of the glacier. Towards the glacier terminus, the thinning rate reaches positive values again.

The thinning rates of the Bechung (**fig. 13b**) show more spatiotemporal variation than the G528. Between 1975 and 2000, the annual thinning rate was nearly balanced (-0.04 m/yr). Towards the terminus, the thinning rate increased to approximately -1 m/yr after which it decreased again at the front. From 2000 to 2017, the glacier thinning was already much higher compared to 1975-2000, at -0.99 m/yr. An increase downslope can be observed, with values around -1.5 m/yr at the terminus. From 2017-2022, the thinning rate fluctuates around 0 m/yr in the higher regions of the glacier. At the glacier front, the annual thinning rate rises to almost -7 m/yr. The average thinning rate from 2017-2022 is -1.15 m/yr.

The Raphsthreng glacier (**fig. 13c**) shows similar characteristics as the Bechung glacier, with an increasing annual thinning rate of -0.45, -0.78 and -1.35 m/yr for 1975-2000, 2000-2016 and 2017-2022 respectively. For all three periods, the thinning rate remained stable for the first 1500 m, with only an increase towards the terminus. In the period 2017-2022, the thinning rate reached a maximum at the glacier front, with values over -8 m/yr, whereas the thinning rate at the front for 1975-2000 and 2000-2017 were -2 and -1 m/yr, respectively.

During its land-terminating phase, the Thorthormi (**fig. 13d**) has shown a constant annual thinning rate of around -0.32 m/yr in 1975-2000, with positive values upslope and at the terminus, and a slight increase at 3000-4000 m of -1.3 m/yr on the flat terminus. The period 2000-2017 already included several years of the lake-terminating Thorthormi, and the thinning rates can be seen to increase to -0.67 m/yr, with the highest values occurring between 2500 and 3500 m, corresponding to the sharp decrease in slope. However, towards the terminus, the thinning decreases again. From 2017-2022, the thinning rapidly increases on the glacier tongue, reaching almost up to -10 m/yr. The average thinning rate in this period amounts up to -0.77 m/yr. The map in **figure 13** shows that the whole glacier tongue, which disappeared in 2022, is subjected to glacier thinning. Also the area marking the transition from a steep to shallow slope is characterized by high thinning values from 2017 to 2022. Between 1975-2022, the first 1500 m of the Thorthormi experiences little thinning, as the values fluctuate around 0 m/yr.

The Lugge glacier (**fig. 13e**) already showed relatively high thinning rates between 1975 and 2000 at the terminus of over -2 m/yr. The upper part of the glacier was still characterized by glacier thickening, as the thinning rate was positive. The average annual thinning rate for 1975-2000 is -0.42 m/yr. The average annual thinning rate for 2000-2017 was -0.55 m/yr and shows a sudden increase around 2500 m to the glacier front from -0.5 to -3.7 m/yr. For 2017-2022, the thinning increased even further to -0.64 m/yr. The terminus has seen an even larger thinning of up to -5.7 m/yr in this period, corresponding to a large region on the glacier terminus. stretching for almost 800 m along the flowline. Note the small decrease in thinning right before the glacier front from -4.8 to -4.2 m/yr. The upper part of the Lugge glacier, to 2000 m, remained relatively constant over the years.

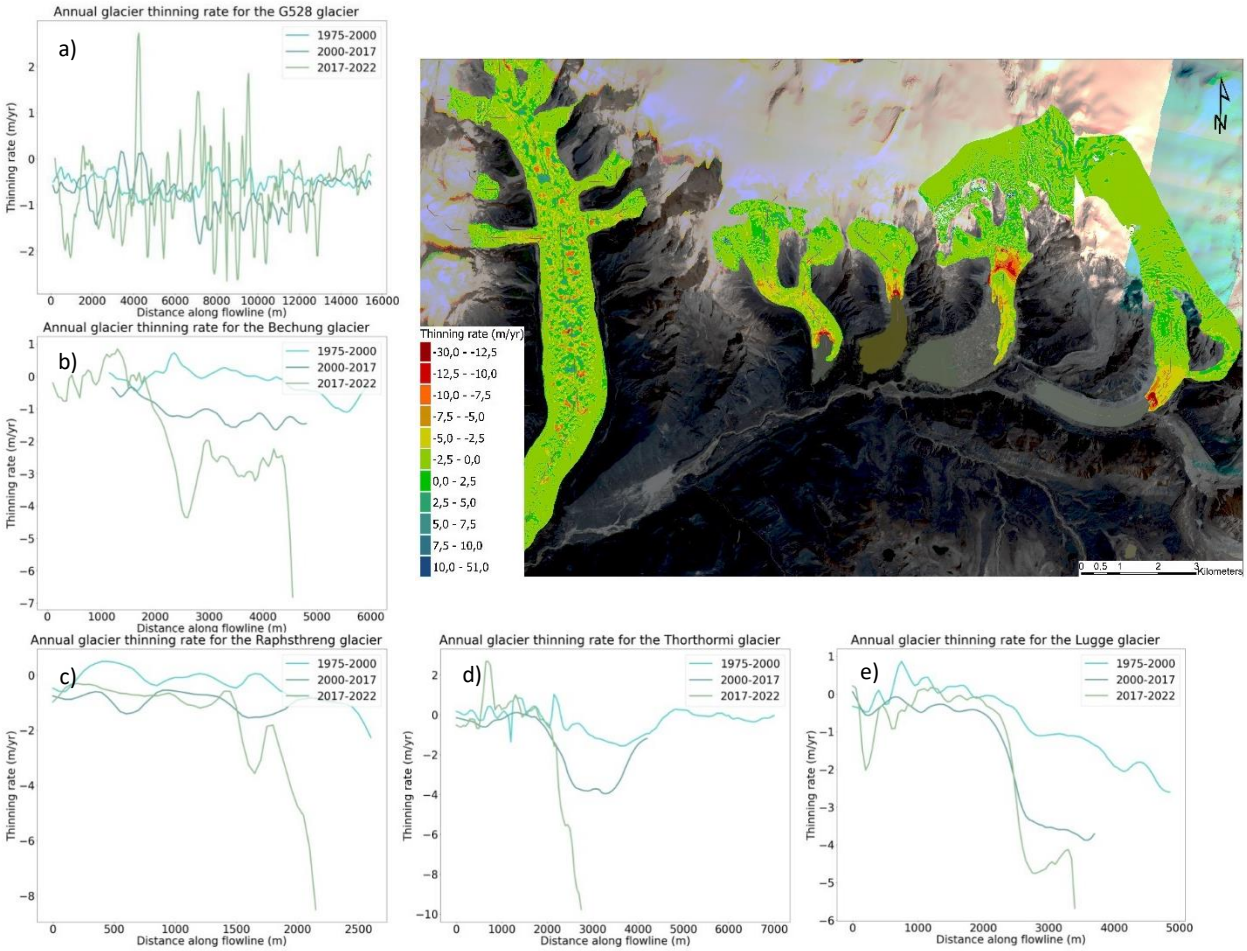

Fig. 13. *The graphs show the annual mean thinning rate (m/yr) along the flowline between 1975 and 2022 for the Lugge glacier, averaged at 50 m intervals. The map shows the spatial variation in thinning rate of the corresponding glaciers between 2017 and 2022. The map is underlain by a PlanetScope image from 2023.*

The annually averaged glacier mass balance for the whole glacier and total glacier mass change between 1975 and 2022, for the three defined periods are shown in **figure 14**. For every consecutive period, the mass balance has become more negative, especially for the Bechung glacier. The Raphsthreng shows the most negative mass balance between 2017 and 2022. All glaciers also showed an increasing mass loss over the years. An exception is the Thorthormi glacier, which lost more mass annually between 2000-2017 than in 2017-2022, 6.85 and 6.68 Mt/yr, respectively. The corresponding statistics for each glacier can be found in **table A5.1–A5.3**.

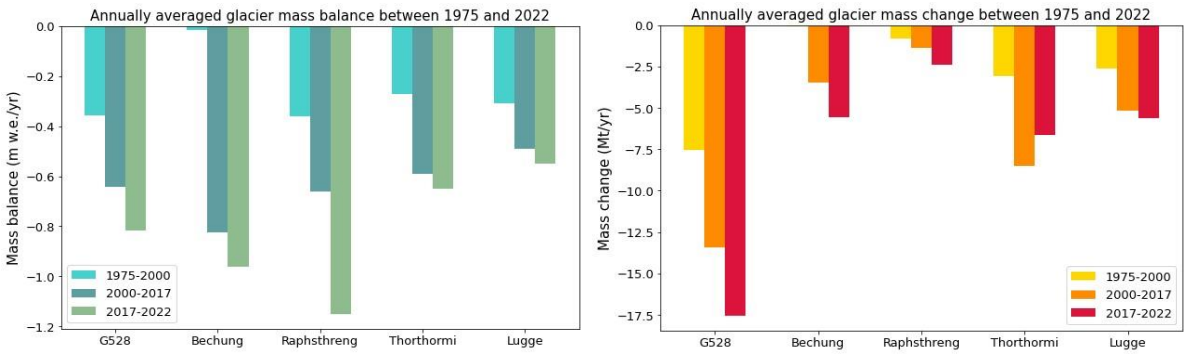

Fig. 14. *The left bar plot shows the annually averaged mass balance between 1975 and 2022 in m/yr for each glacier. The bar plot on the right shows their corresponding mass change in Mt/year.*

6. Discussion

6.1 Forces and processes controlling land- and lake-terminating glaciers

6.1.1 Glacier dynamics, climate and general patterns in flow velocity and thinning

The driving stress of glacier flow is driven by the gravitational acceleration, ice thickness, surface slope and ice density. A slope gradient arises through accumulation upslope and ablation downslope, which increases the driving force [Jiskoot, 2011]. The higher surface flow velocities observed on the glaciers in this study can therefore mainly be explained by the slope, where a steeper slope coincides with higher flow velocities. The driving stress is balanced by resistive stresses, which mainly comprise basal drag and lateral drag. Basal drag is the main resistive force, acting at the base of the glacier where it slides over the bedrock. Lateral drag is the resistance a glacier experiences from the valley walls [Jiskoot, 2011; Marshall, 2011]. When the slope decreases, the flow velocity decreases, as the resistive stress increases relative to the driving stress. This explains the generally observed decrease in flow velocity near the glacier front compared to steeper regions. A transverse velocity profile confirms this as the velocity decreases towards the edges of the glacier, indicating a large enough lateral drag to decrease the velocity downslope. The higher regions of the glaciers mainly exhibit lower flow velocities than downstream, corresponding to the accumulation zone where ice moves slower and primarily in the vertical direction.

The temperature in Lunana has increased with 1.1 °C (+0.0256 °C yr^{-1}) between 1979 and 2023 with significantly warmer years in the past two decades (**fig. 15**). The observed increase in glacier thinning can therefore be partly explained by the increase in air temperature [Bhattacharya et al., 2023; IPCC, 2021]. The minimal change in thinning between 1975 and 2022 at higher elevations illustrates that the increase in temperature has a limited impact on higher altitudes. However, when coupled with the effect from lakes, it heavily affects the lower regions of the glaciers as they experience significant thinning. It is however important to note that for the period 2017 to 2022 (**fig. 13**), the sharp increase in thinning rate, frequently observed at the glacier front, might also represent calving processes and the presence of icebergs rather than the actual thinning rate. These observations remain however speculative, but the decision was made to show them rather than to discard them. Overall, the thinning of the land-terminating G528 glacier is much lower (+1.5 to -2.5 m/yr) than those of the lake-terminating glaciers (-2.5 to -7.0 m/yr) at equal altitudes. This difference arises because the impact of increasing air temperatures is overshadowed by the influence of calving processes on the termini of lake-terminating glaciers (section 6.2.3).

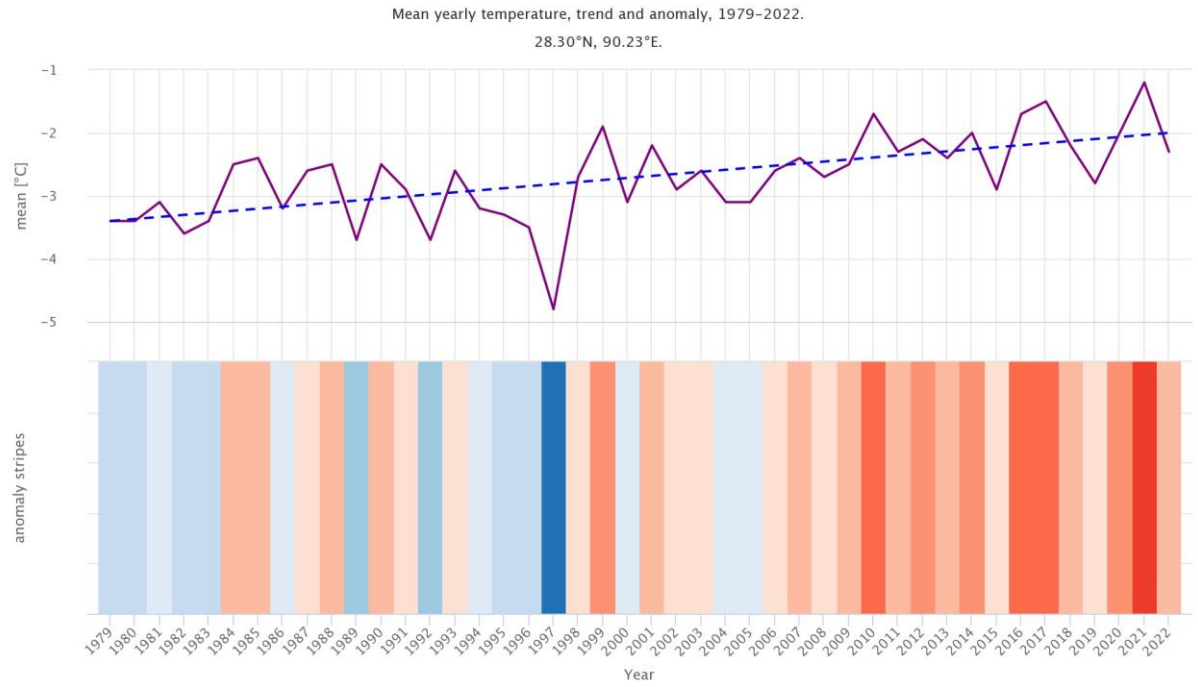

Fig. 15. *Graph showing the mean annual temperature in the Lunana region between 1979 to 2022. The anomaly stripes present a visual interpretation of the graph of the average annual temperature, where red stripes indicate periods of higher temperatures and blue stripes, lower temperatures relative to the mean [from: MeteoBlue].*

6.1.2 Supraglacial lakes, climate forcing and glacier response

The temporal changes in mean supraglacial lake area and number on G528 are illustrated in **figure 16**, which excludes Landsat data. The left graph shows an increase in supraglacial lake area (+53.6 m^2/yr on average), generally with extremely fluctuating values. However, the highest values occur in the most recent years. The right graph shows a general decrease in supraglacial lake number. Both graphs including Landsat imagery show contrasting trends (**fig. A6**). Due to its low resolution it failed to detect many smaller lakes, and it only considered the large lakes resulting in a higher mean area and low number of lakes between 2003 and 2008.

Multiple studies have shown increases in supraglacial lake area and number in HMA as a response to increases in air temperature [Jian et al., 2018; Komori, 2008; Song et al., 2016; Veettil et al., 2016], also observed in the Lunana region, and precipitation, causing intensified lake filling and drainage [Wendleder et al., 2018; Wendleder et al., 2021]. The precipitation rate in Lunana has increased by 122.1 mm between 1979 and 2022 (+2.84 mm/yr), which mainly increased in spring and summer (**fig. A7** & **A8**). It is therefore likely that the lake area on the G528 glacier has increased through rising air temperature and increased precipitation. However, the number of supraglacial lakes has been decreasing. Satellite observations on the G528 glacier have shown that smaller lakes coalesce, decreasing the number of lakes, and subsequently increasing the lake area. The observed fluctuations in the data might be the result of seasonal variations between years, ice cover and atmospheric noise, considering the notable data spread.

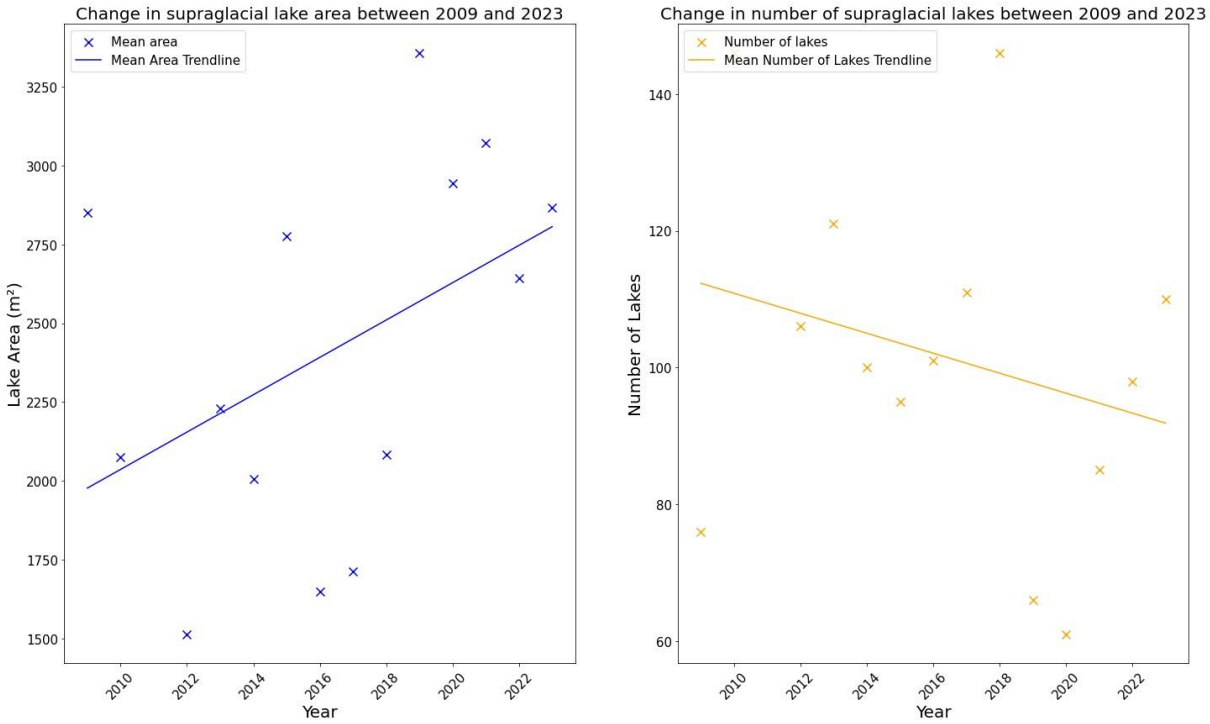

Fig. 16. *The graph on the left shows the mean change in supraglacial lake area between 2009 and 2023. The graph on the left shows the mean change in number of supraglacial lakes between 2009 and 2023. The figure including the Landsat data from 2003 to 2008 is presented in* **fig. A6**.

The observed increase in velocity between 2017 and 2022 on the G528 glacier might be attributed to the increased drainage of the lakes to the glacier bed, reducing the effective pressure and enhancing basal sliding [Wendleder et al., 2021]. However, additional research is necessary to fully attribute the increase in supraglacial lakes to the observed acceleration, since these lakes do not necessarily contribute to an annual increase in velocity, but rather seasonal speed-ups. Besides changes in air temperature, glacier thinning might also be affected through the presence of supraglacial lakes by decreasing the overall albedo of the glacier and by absorbing incoming solar radiation, which further promotes thinning through a positive feedback [Benn et al., 2012; Gardelle et al., 2011; Stokes et al., 2019]. Moreover, the annual mass loss of G528 has more than doubled in 2017 to 2022, compared to 1975 to 2000 (-17.57 and -6.56 Mt/yr, respectively) as the total area remained constant. This indicates that the glacier experiences significant vertical loss mainly through supraglacial lake formation [Benn et al., 2012]. Increased air temperatures also caused supraglacial lakes to propagate to higher elevations (**fig. A9**), as is also widely observed on Greenland glaciers [Gledhill & Williamson, 2018; Leeson et al., 2015]. At the terminus of G528, low thinning rates are observed. From satellite images it is observed that the glacier front is heavily covered by debris, and vegetation appears to grow on the lateral parts of the tongue. The presence of debris, combined with the low number of supraglacial lakes in this zone (**fig. A9**), might indicate that the ice underneath is isolated by a thick layer of debris, and therefore shows minimal thinning. The extremely fluctuating thinning rates from **fig. 13** can be explained by the displacement, drainage and appearance of supraglacial lakes over the years.

The occurrence of supraglacial lakes on the G528 could be an indicator of the formation of a proglacial lake in the future [Benn et al., 2012], although the supraglacial-lake-phase could take up to 40 years [Komori, 2008]. During the 1990s to early 2000s, the Bechung glacier featured multiple large supraglacial lakes, which merged together to form a large glacial lake, currently developing into a proglacial lake [Wangchuk et al., 2022]. The glacier experiences massive increases in annual mass loss in 2000-2022 compared to 1975-2000 (-5.50 to -0.12 Mt/yr, respectively). Still nowadays, the Bechung

glacier shows a significant number of supraglacial lakes on its surface, which contributes to glacier thinning and might promote the rapid expansion of lake in front of the glacier [Benn et al., 2012; Sakai et al., 2009].

6.1.3 Proglacial lake expansion: crevasse formation, iceberg production and calving

Over the past two decades, the lakes in front of the Bechung, Raphsthreng, Thorthormi and Lugge glacier have undergone significant expansion corresponding to increased glacier mass loss. Whereas the proglacial lakes of Raphsthreng and Lugge have existed for several decades already [Komori, 2008], the Thorthormi and Bechung glacier have only developed a proglacial lake over the past 20 years. This section discusses the occurrence of crevasses on the Bechung, Raphsthreng and Lugge glacier, and the formation of icebergs in their lakes. These two features can give an indication on the dominant calving processes for each glacier which influence flow velocity, thinning rate and glacier retreat. The disintegration of the Thorthormi glacier will be discussed separately.

Crevasses form as the elastic threshold of glacier ice is exceeded and the ice fractures, which is common on fast-moving glacial regions. Their occurrence can provide insight in the ice dynamics at that specific part of the glacier [Colgan et al., 2016; Herzfeld et al., 2004]. Transverse crevasses, perpendicular to the flow direction, occur in regions where the ice is stretching, for example on steep slopes (**fig. A10**). At the sides of the glaciers, marginal crevasses can form through lateral drag. At the glacier front, longitudinal crevasses are present due to the compression of ice (**fig. 17**). Transverse and marginal crevasses are observed on all glaciers in this study. However, the glaciers in this study show transverse crevasses at the glacier front instead of longitudinal crevasses, indicating stretching of the ice.

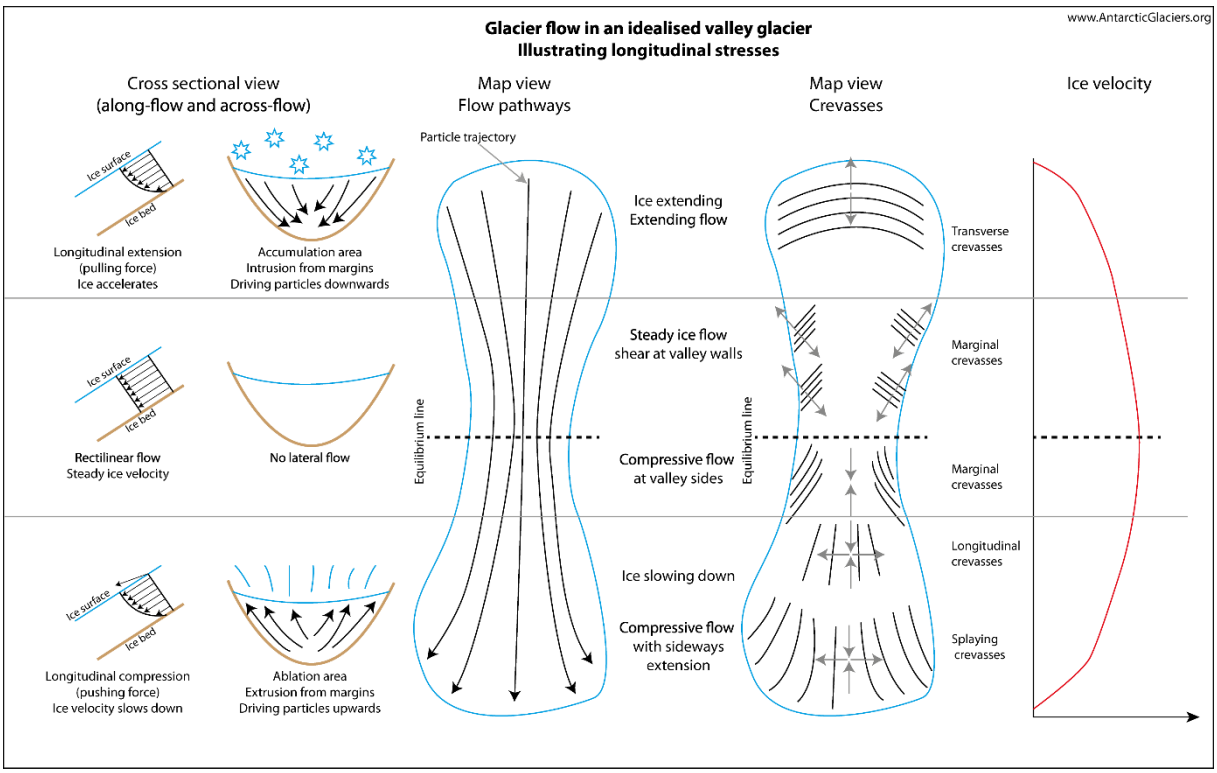

Fig. 17. *Schematic overview of an idealized valley glacier showing the occurrence of crevasses on different parts of the region subjected to factors as compression, stretching and lateral drag [from: www.AntarcticGlaciers.org].*

At the glacier front, crevasses can promote calving through crevasse propagation. This process is influenced by tensile and compressive stresses, the ice overburden pressure and hydrofracturing [Van der Veen, 1998]. Hydrofracturing can counteract the ice overburden pressure, thereby penetrating the

ice deeper [Benn et al., 2009]. Crevasse propagation is a crucial process for calving by significantly weakening the ice, facilitating calving along these lines of weakness through buoyant uplift, subaqueous melt and thermal notching [Benn et al., 2007; Colgan et al., 2016]. The Bechung and Raphsthreng glaciers are characterized by a small region of transverse crevasses at the glacier front. This indicates that their termini are stable, which makes them less prone to calving compared to glaciers with heavily crevassed fronts [Colgan et al., 2016]. Crevasse propagation can also be the result of dynamic thinning causing increased thinning near the terminus. The development and expansion of a proglacial lake decreases basal drag, resulting in an acceleration of the glacier terminus [Sato et al., 2022]. The stretching resulting from this acceleration leads to an increased glacier thinning which can promote flotation [Tsutaki et al., 2013]. Additionally, the tensile stresses in the ice open up transverse crevasses making the glacier front more prone to calving. Ultimately, dynamic thinning leads to frontal retreat through significant mass loss from calving and surface thinning, which starts a positive feedback loop by reducing resistive stresses at the front leading to further calving [Ben et al., 2007; Nick et al., 2013]. The Bechung and Raphsthreng glacier show a significant decrease in flow velocity compared to their upglacier regions, and the velocities can be seen to decrease over the years. In addition, their thinning rates only increase significantly close to the front, suggesting that their termini are not affected by dynamic thinning. In contrast, the Lugge glacier exhibits an acceleration towards its terminus, with substantial increases in velocity over time and a large region (800 m) of high thinning values, corresponding to the large area of transverse crevasses. This suggests that its terminus is affected by dynamic thinning.

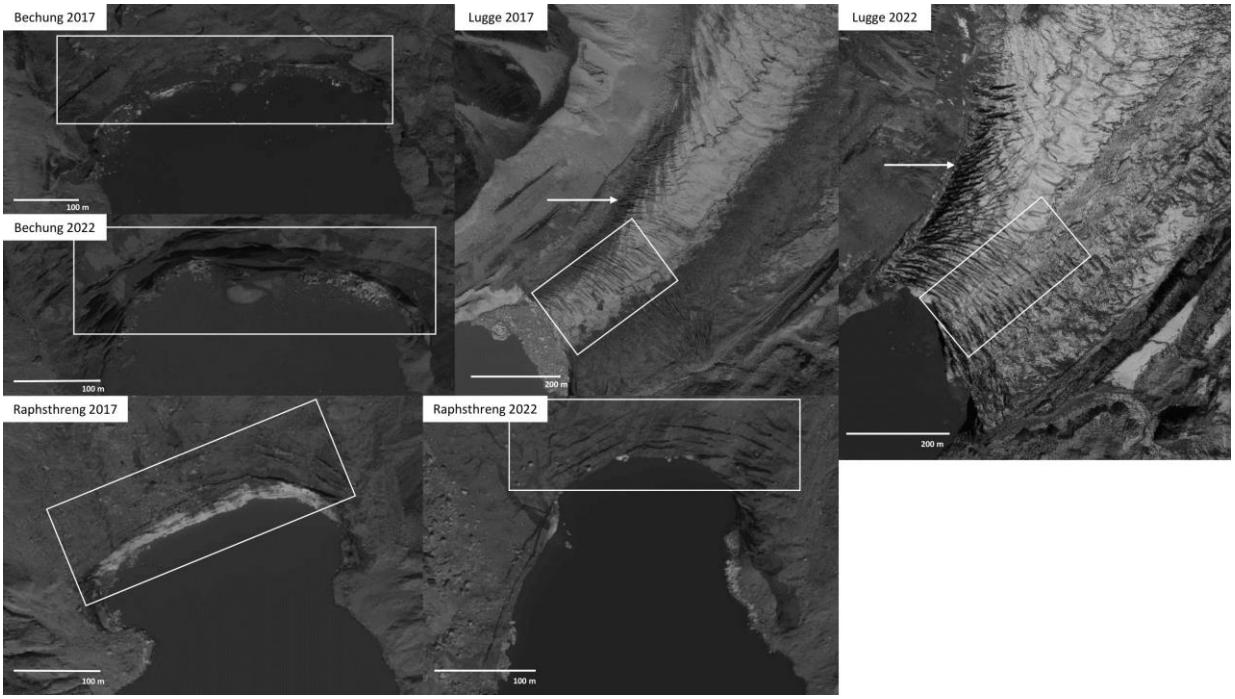

Fig. 18. *Pléiades images showing the glacier fronts of the Bechung, Raphsthreng and Lugge glaciers in 2017 and 2022. The white boxes show some of the transverse crevasses present at the front, whereas the arrows indicate some marginal crevasses on the Lugge glacier. The resolution of the images is 0.5 m.*

Calving at the glacier front leads to the formation of icebergs, whose size and number in a lake can provide insight on the dominant processes driving calving. Large, tabular icebergs are mainly driven by buoyancy. The thinning of the glacier terminus makes it more vulnerable for flotation, and along with deeply penetrating crevasses this can result in buoyancy-induced calving, producing large icebergs [Minowa et al., 2023]. Smaller icebergs are produced through thermal undercutting and notching at the waterline [Röhl, 2006].

The small size and low number of icebergs in the glacial lakes of Bechung and Raphsthreng (**fig. 19**), combined with the few crevasses along the glacier front and the relatively low, decreasing flow velocities on the glacier terminus indicate that their glacier retreat and calving is mainly dominated by subaqueous melt and thermal notching which undercut the subaerial ice [Röhl, 2006; Truffer & Motyka, 2016]. In addition, the decreasing flow velocities on the termini of Bechung and Raphsthreng suggest that the flow velocity is mainly affected by a reduction in driving stresses through a decrease in ice thickness. Moreover, due to the presence of stagnant "dead-ice" in the Bechung glacial lake, it is hypothesized that there is still ice present underneath its lake, which has not been removed yet. The low velocities observed on the terminus might indicate that the presence of subaqueous ice possibly provides a buttressing effect. Due to the likely presence of ice underneath the Bechung lake, the lake can not be conclusively classified as a fully developed proglacial lake, but rather as a base-level lake according to Benn et al. (2001). The Raphsthreng glacier is characterized by periods of glacier advance. One of those periods is highlighted in **fig. A11**. At the glacier front, an ice-mélange is present, being enclosed by an ice bridge. It is hypothesized that this ice-mélange, being kept in place by the geometry of the glacier snout, exerts a cooling effect on the region leading to the closing of the ice bridge around the mélange. The ice-mélange, now being isolated from the rest of the lake, controls the calving of the glacier by providing a supportive stress (buttressing) which enables the glacier to advance [Amundson et al., 2010].

The icebergs in the Lugge glacial lake are both larger and more numerous than the icebergs in the Bechung and Raphsthreng lakes. It is hypothesized that several processes affect the calving at the front of Lugge through complex interactions which might explain the observed differences in crevasses and icebergs between the Lugge and the other two glaciers. Thermal undercutting and thermal notching contribute to the calving of smaller icebergs similar to Bechung and Raphsthreng. In addition, hydrofracturing causes crevasses to expand and penetrate the glacier, promoting calving by weakening the ice. A large region of transverse crevasses near the glacier front, in combination with periods of substantial production of large-sized icebergs, significant thinning (at -5 m/yr) and observed acceleration over the past five years at the glacier terminus can be an indication of dynamic thinning. The periodic increases in iceberg production can imply buoyancy-driven calving at the glacier front as dynamic thinning and hydrofracturing cause slight buoyant uplift of the terminus, producing larger, tabular icebergs [Boyce et al., 2007]. An indication of this buoyant uplift is apparent in the final 400 m of the glacier thinning rate from 2017-2022 (**fig. 13**) as the buoyant uplift offsets glacier thinning. This region corresponds to the heavily crevassed region. In addition, Tsutaki et al. (2019) found that 88% of the thickness of the Lugge was submerged in 2001, and Lugge would rapidly retreat should the ice flotation level be reached.

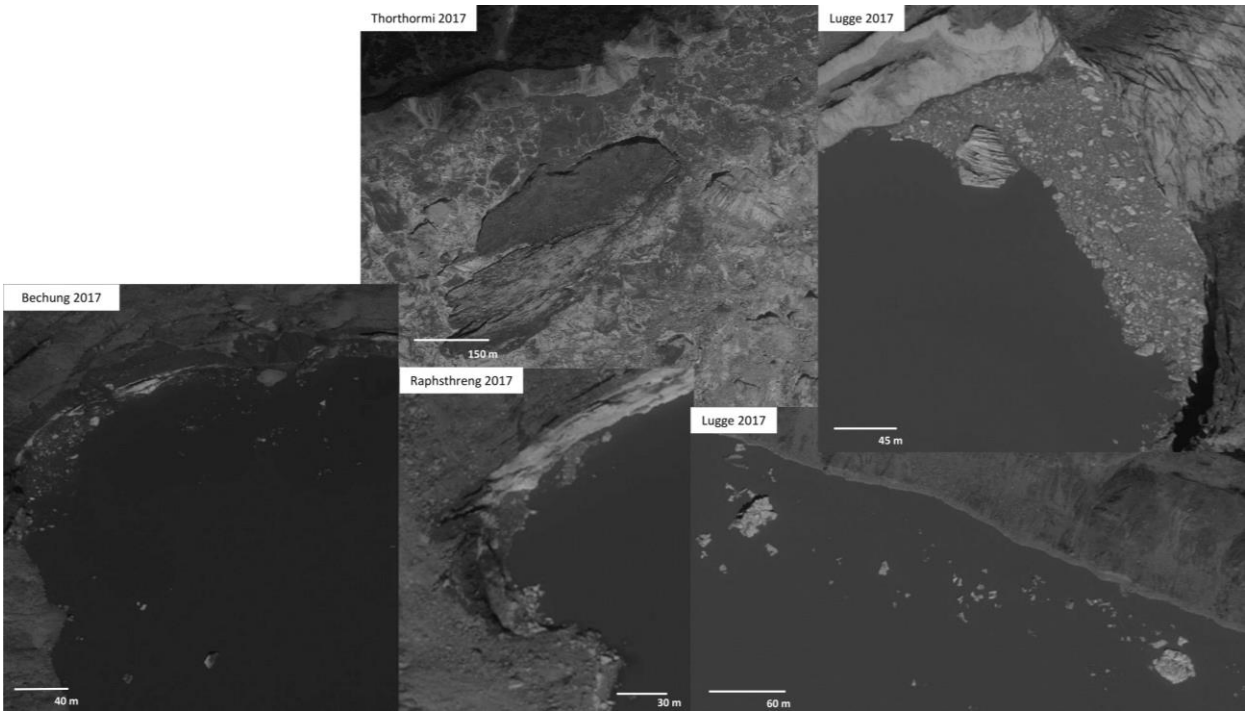

Fig. 19. *Pléiades images showing examples of icebergs in the proglacial lakes of the studied glaciers in 2017. The Thorthormi proglacial lake is also incorporated in this figure to highlight its mélange, with extremely large icebergs compared to the other glacial lakes. The resolution of the images is 0.5 m.*

The Thorthormi glacier has shown the most development over the past 20 years, in terms of lake expansion, flow velocity and glacier thinning. In 2003, the Thorthormi glacier was still in contact with the terminal moraine. The surface was already spotted with multiple large lakes which expanded over the following years, only to gradually merge with the lateral glacial lakes. However, these supraglacial lakes did not result in enhanced thinning at the glacier snout, since the terminus was subjected to longitudinal compressive stresses, balancing the thinning by the lakes [Tsutaki et al., 2019]. After the lake decoupled from the terminal moraine in 2011, the stress regime changed from compressional to extensional, and due to enhanced basal sliding, the flow velocities increased. Nevertheless, the flow velocities did not increase substantially until 2016, indicating that the glacier was still in contact with the subaqueous moraine [Sato et al., 2022]. From 2016, the flow velocities increased. The lakes at the side of the glacier reduced the lateral drag, which accelerated the glacier terminus. This enhanced the ice flux towards the terminus, leading to increased calving in a positive feedback loop. Through the substantial dynamic thinning of the glacier surface over the years, the terminus became buoyant around 2017 [Sato et al., 2022]. From this point, the glacier can be seen to accelerate through dynamic thinning and hydrofracturing, leading to the formation of massive crevasses on the margins of the tongue, which rapidly propagated to the center of the glacier. As a result, the terminus rapidly lost mass through buoyancy-induced calving, releasing large tabular icebergs up to over 500 m in diameter. In 2022, the glacier retreated on the steep slope adjacent to the lake, where it has stabilized. The glacier front is characterized by a large region of transverse crevasses which still actively calves into the ice mélange of the proglacial lake (**fig. 20**). Important to note is that the mass loss of Thorthormi decreased in 2017-2022 relative to 2000-2017. As the area substantially decreased with the disappearance of the floating tongue, the mass loss decreased as well (eq. 7).

The observed velocity decrease in 2017 and 2020 on the ground-based part of the Thorthormi right before the glacier tongue can be attributed to the backstress or buttressing that the floating tongue exerts on the glacier. After the tongue disappeared in 2022, a significant increase in velocity can be observed in the same region of the glacier. Furthermore, the ice mélange, a mixture of lake ice and

icebergs produced by calving, can also buttress the glacier and control calving events [Amundson et al., 2010; Dupont & Alley, 2005; Geirsdóttir et al., 2008]. However, since this mechanism is season-dependent, and individual calving events can hardly be observed with satellite imagery it would require in-field observations to determine the contribution of the ice mélange or lake ice.

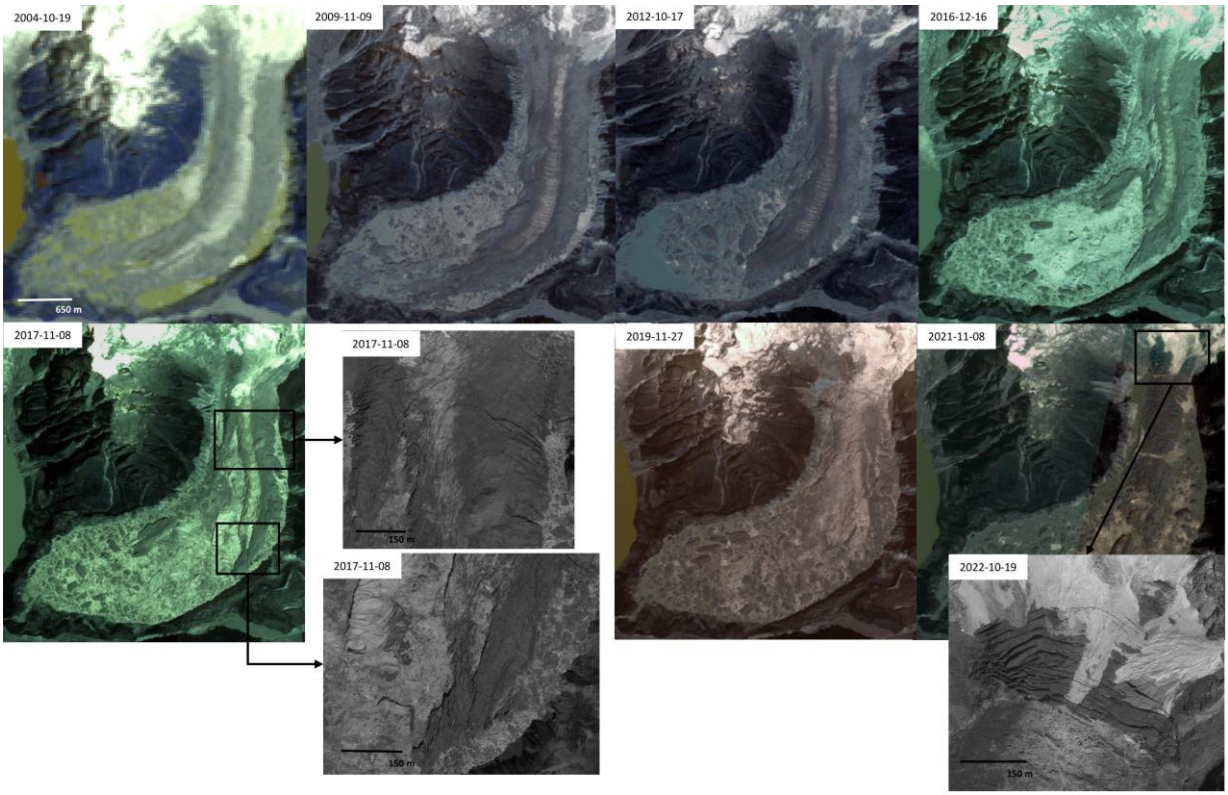

Fig. 20. *Timeseries of satellite images applied in this study which shows the development of the Thorthormi glacier, where some regions in 2017 and 2022 are highlighted by using Pléiades imagery (0.5 m resolution). Note that after 2017, the glacier tongue rapidly disintegrates through buoyant uplift and crevasse propagation. The glacier front is currently characterized by a large region of transverse crevasses.*

6.2 Literature comparison

In general, the glacier velocities produced in this study show many similarities to the available literature but also yield interesting distinctions. A study by Millan et al. (2022) applied several feature tracking tools to map the flow velocity of the total global glacier area between 2017 and 2018 at 50 m resolution. It accurately follows the velocities of the G528 and Bechung presented in this study, and partly underestimates the Raphsthreng velocity relative to this study. The velocities of Thorthormi and Lugge show few similarities to Millan et al. (2022), as they showed velocities at Thorthormi between 1000 and 2000 m to reach up to 350 m/yr, where this study revealed velocities around 20 m/yr, and the Lugge showed much higher velocities (between 200 and 300 m/yr) compared to the velocities presented in this study. Kääb (2005) studied the velocities on the G528 glacier from 2001 to 2002 using the CIAS tool. Their velocities correspond in magnitude and trend to the Landsat velocities from 2006 presented in this study. Tsutaki et al. (2019) used the COSI-Corr software to track the surface displacement of the Thorthormi and Lugge glacier from 2002 to 2010. The velocities at the Thorthormi glacier show high correlation to the velocities from 2006 in this study, although the velocities produced by Tsutaki et al. (2019) are slightly higher. Near the terminus of the Lugge glacier, their velocities also show high correlation to the velocities presented in this study, however on the steeper part, the velocities suddenly drop to 5 m/yr, whereas this study found values to over 100 m/yr for the same

region in 2006. COSI-Corr and GIV track glacier features inside a spatial search window over time, calculating the displacement. If the images are too far spaced in time relative to the flow velocity, the data may lose coherence as the software fails to track the same glacier features over time as the features can disappear or move outside the search window [Van Wyk de Vries & Wickert, 2021]. For Tsutaki et al. (2019), the temporal resolution of the input data varied between one and two years making it too coarse to track the same features over time on the fast-moving region. Therefore, the velocity measurements on the Lugge glacier are largely underestimated which explains the large differences relative to this study. Sato et al. (2022) used the ImGRAFT feature tracking tool to estimate the flow velocities of the Thorthormi and Lugge from 2016 and 2017. The velocities of the Thorthormi are relatively comparable to this study, with high velocities (up to 200 m/yr on the tongue) and decreasing velocities on the ground-based part through buttressing. The velocities on the Lugge are comparable to the study by Tsutaki et al. (2019) with a sharp decrease on the steepest part of the glacier to 5 m/yr. Sato et al. (2022) also used a coarse temporal resolution (1-year gap) relative to the flow velocity in this region. The ITS_LIVE velocity dataset, automatically derived by importing Landsat imagery in the auto-RIFT tracking tool, was evaluated for the Thorthormi and Lugge for 2010-2018 by Sato et al. (2022). For 2013, ITS_LIVE showed relatively high comparison in trend and magnitude to the velocities generated in this study. However, in 2017 they showed a large deviation at the glacier tongue, with velocities ranging from 5 to 10 m/yr, compared to over 250 m/yr for this study. For the Lugge, the ITS_LIVE showed velocities below 5 m/yr for the whole glacier for 2010-2018. The differences of the ITS_LIVE dataset are likely attributed to the coarseness of the resolution (240 m) compared to this study.

The average annual thinning rates produced by Tsutaki et al. (2019) and Sato et al. (2022) for the Thorthormi and Lugge glacier were significantly higher compared to this study (-1.40 and -4.67 m/yr for 2004-2011, respectively [Tsutaki et al., 2019] and -2.78 and 2.87 m/yr for 2011-2018, respectively [Sato et al., 2022]). The large differences arise as both studies measured the thinning rates only at the glacier terminus, whereas this study computed the average thinning rate across the whole glacier, including the accumulation zone. The inclusion of the accumulation zone, where thinning rates are lower, leads to an lower average thinning rate compared to the average thinning rate for the ablation zone only, where glacier thinning is higher. Furthermore, it remains unknown whether the sharp increase in thinning rate observed at the glacier front is through actual thinning or through calving-related processes. Sato et al. (2022) however also reports high thinning values on the glacier terminus of up to -5 m/yr for both Thorthormi and Lugge.

Thickness data was extracted from Farinotti et al. (2019), who used an ensemble of five glacier models to simulate the glacier thickness, and Millan et al. (2022), who used the Shallow Ice Approximation, implementing flow velocities from the results of feature tracking software, and calibrating the model with field measurements from the GlaThiDa. Both studies showed an increase of ice thickness towards the glacier terminus, except for the G528 glacier (**fig. A12**). Since glacier thickness drives glacier flow, higher velocities would be expected due to this increase in thickness. However, the velocities mainly decrease towards the terminus. This could indicate that internal deformation (or ice creep) is the dominant process here instead of basal sliding [Jiskoot, 2011]. However, due to the global scale of the studies, the simplicity of glacier models and the lack of representable local measurements, the glacier thickness and the effect it has on the glacier dynamics in this region remain highly speculative.

6.3 Uncertainties, assumptions and improvements

The main uncertainty arises from the use of Landsat imagery. For the lake detection, the Landsat images yielded the largest relative error (ranging from 5 to 43%; **tab. A4.1-A4.4**). Moreover, Landsat was also unable to recognize many smaller supraglacial lakes on G528. In comparison, RapidEye and PlanetScope images yielded an extremely low relative error (1% and 0.5%, respectively). The velocities in 2006 and 2013 showed significantly lower values in the high velocity regions of the glaciers compared to 2017 to 2022. This could indicate massive glacier dynamic changes for all glaciers, or the inability of Landsat imagery to track glacier features over time. The latter seems more probable due to the relatively coarse temporal coverage (often more than a 3 week gap) combined with the coarse spatial resolution (30 m) and relatively small glacier area. The trends of the Landsat imagery correspond to the available literature which also made use of low resolution imagery. Additionally, it is important to note that the thinning rate from 1975 to 2017 might also be underestimated due to the coarser resolution of the data compared to 2017-2022 resulting in less negative values, especially near the calving front. Therefore, this study has shown that higher resolution is more reliable and that Landsat, and other low resolution imagery are not suitable for relatively small glaciers but can show promising results on larger glaciers.

Another uncertainty is the use of the feature tracking tool GIV, due to its recent development and limited application in research. To evaluate the accuracy of GIV, velocity measurements in the field should be conducted. Nevertheless, this study yielded promising flow velocity results which often corresponded closely to similar studies which used different, widely-applied, feature tracking tools. Therefore, the application of GIV in this study appeared as a convenient, rapid method of deriving surface flow velocities, along with the potential of producing high accuracy velocity maps. In addition, the velocities and thinning rates along the flowline were buffered to eliminate outliers in the data. Nevertheless, this buffering resulted in a slight underestimation of the velocities at the flowline, as velocities farther from the flowline were also included. This buffering however, simultaneously reduced the robustness of the results.

Certain processes remain speculative, such as the dominant calving processes at the Lugge glacier and the seasonal variation of supraglacial lakes, which are influenced by many other factors. Remote sensing is limited to certain factors as weather, availability of specific sensors and spatiotemporal resolution, whereas glacier modelling is dependent on the accuracy of the input data and knowledge of glacier physics and processes. Therefore, factors like the ice thickness, bedrock morphology, meteorological observations, lake depth, temperature and bathymetry makes fieldwork in this region necessary to get a more accurate understanding on the effect of proglacial lakes on glacier dynamics.

6.4 The future of the Lunana region

The expansion of the proglacial lakes will probably continue in the coming decades under global warming as the glacier mass continues to decrease globally [IPCC, 2021]. The glaciated regions in Bhutan are most affected by climate change and are not even halted by the lowest emission scenarios. For SSP1-2.6, lake area and volume would increase by 9 km^2 and 0.5 km^3 at the end of this century. Under higher scenarios, these values will increase even more, up to 25 km^2 and 2.9 km^3, following SSP5-8.5 [Furian et al., 2022].

Bhutan's glaciated regions are characterized by relatively low amounts of overdeepenings compared to other regions. However, they have a high volume-to-area ratio, indicating the presence of large and deep basins underneath glaciers which can store large amounts of water [Furian et al., 2021]. The overdeepening database of Furian & Wilhelm (2020) showed large overdeepenings underneath the G528, Bechung, Thorthormi and Lugge glaciers, with an average depth of 66, 42, 144 and 60 m,

respectively (**fig. A13**). The proglacial lake of the Thorthormi already fully covers the overdeepening, reaching to where the glacier front is currently located on the steeper slope. The proglacial lakes of the Bechung and Lugge glacier partly fill up the overdeepening, but the glacier still covers part of it. This indicates that the glacier front possible retreats on a reverse bed slope, which can accelerate the glacier flow and make the terminus more prone to flotation leading to accelerated mass loss. The retreat on a reverse bed slope might explain the acceleration observed at the Lugge terminus [Tsutaki et al., 2019]. The lower zone of the G528 also hosts a large overdeepening. The presence and observed increase in supraglacial lakes might indicate the formation of a proglacial lake in the (near) future. Therefore, it is expected that through a combination of increasing air temperatures, merging of supraglacial lakes and the presence of large overdeepenings, the expansion of proglacial lakes is promoted and accelerated.

The risk for glacial lake outburst floods (GLOFs) will increase through the formation and expansion of proglacial lakes in overdeepenings [Furian et al., 2021; Furian et al., 2022]. GLOFs can be triggered through large waves in the lake due to landslides, calving or rockfalls or by the failure of the moraine dam. The Lunana region is very susceptible to GLOFs as the Bechung, Raphsthreng, Thorthormi and Lugge all form a high risk [Rinzin et al., 2021]. Since 1990, there have been numerous GLOFs in this region with the most devastating in 1994 from the Lugge proglacial lake [Watanbe & Rothacher, 1996]. The most dangerous lake in the Lunana nowadays is the Thorthormi proglacial lake, which is separated from the Raphsthreng glacial lake only by an unstable moraine wall. Despite the efforts to lower the water level of the Thorthormi, the lake is still considered dangerous [Singh, 2009]. This has been proven as a GLOF occurred in the lake on October 30, 2023. From satellite imagery (**fig. A14**), it can be observed that an avalanche on the glacier surface possibly generated a wave in the lake which triggered the GLOF. According to the NCHM (National Centre for Hydrology and Meteorology) the ice avalanche, caused by increased air temperatures over the previous weeks, produced a wave of 4 meters high, overtopping the terminal moraine and lowering the lake level by 40 cm. This GLOF is once again an example of the pressing dangers related to glacial lakes and shows the necessity for a clear understanding and close monitoring of these lakes, as well as the implementation of sufficient measures and hazard management for the downstream communities [Rinzin et al., 2023].

Increasing our understanding for proglacial lake development and the effect they have on glacier behavior to take sufficient measures can only be done through in-situ observations to validate the results presented in this study, and to address the multiple unknown factors regarding lake and glacier interactions and processes.

7. Conclusion

In this paper, the development of proglacial lakes in the Lunana region and the effect of these lakes on glacier velocity and thinning rates is presented. The study was revolutionary as it applied high resolution imagery and a newly developed, convenient and rapid method to derive glacier surface flow velocities. The results showed that the glacial lakes have experienced rapid expansion over the past two decades, heavily affecting glacier flow velocity and thinning rates. Rising air temperatures over this period also contributed to enhanced glacier thinning, and possible changes in their flow velocities. Nonetheless, lake-terminating glaciers are characterized by much higher flow velocities and thinning rates compared to land-terminating glaciers. However, large differences in flow velocity and thinning rates were observed between lake-terminating glaciers due to different dominant processes at the lake-ice boundary. Since the decoupling from the terminal moraine in 2011, the Thorthormi rapidly retreated through dynamic thinning, promoting flotation of the terminus, and consequently buoyancy-induced calving. In 2022, the glacier retreated on a steep slope where it actively calves into the lake with high flow velocities. The Lugge terminus has experienced acceleration over the past years as a result of dynamic thinning leading to increased calving at the glacier front through a positive feedback.

A combination of subaqueous melt, hydrofracturing and buoyant uplift resulted in periods of increased mass loss. On the other hand, the Bechung and Raphsthreng glaciers are less affected by their lakes, as they showed decreasing flow velocities over time implying a decrease in driving stresses through glacier thinning. For these glaciers, subaqueous melt and thermal notching are the dominant processes at the front leading to calving. The land-terminating G528 glacier showed an increase in supraglacial lake area due to increasing air temperatures. These lakes expand and merge, promoting glacier thinning by decreasing the albedo of the glacier through a positive feedback. It is expected that in the future a proglacial lake will form through the continuous merging of supraglacial lakes and the presence of an overdeepening underneath the glacier. The glaciers in the Lunana region, and throughout HMA, are expected to continue to lose mass in the future at high rates through multiple positive feedback loops associated with global warming, lake expansion and the gradual emergence and filling of overdeepenings.

To conclude, proglacial lakes might affect their glaciers by increased flow velocities through dynamic thinning and buoyant uplift, leading to enhanced thinning rates and mass loss through calving. However, the response of each glacier to its proglacial lake can vary significantly, depending on numerous known and unknown factors including lake bathymetry and ice thickness. Therefore more research, and especially fieldwork, is needed to study these diverse processes and interactions. Furthermore, as the risks for GLOFs in mountainous regions increase, the need for monitoring these lakes and increasing our knowledge on its dynamics was never higher.

References

- **Ageta**, Y., & Higuchi, K. (1984). Estimation of mass balance components of a summer-accumulation type glacier in the Nepal Himalaya. *Geografiska Annaler: Series A, Physical Geography*, *66*(3), 249-255.
- **Ahn**, Y., & Howat, I. M. (2011). Efficient automated glacier surface velocity measurement from repeat images using multi-image/multichip and null exclusion feature tracking. *IEEE Transactions on Geoscience and Remote Sensing*, *49*(8), 2838-2846.
- **Amundson**, J. M., Fahnestock, M., Truffer, M., Brown, J., Lüthi, M. P., & Motyka, R. J. (2010). Ice mélange dynamics and implications for terminus stability, Jakobshavn Isbræ, Greenland. *Journal of Geophysical Research: Earth Surface*, *115*(F1).
- **Bajracharya**, S. R., Maharjan, S. B., & Shrestha, F. (2014). The status and decadal change of glaciers in Bhutan from the 1980s to 2010 based on satellite data. *Annals of Glaciology*, *55*(66), 159-166.
- **Benn**, D. I., Wiseman, S., & Hands, K. A. (2001). Growth and drainage of supraglacial lakes on debris-mantled Ngozumpa Glacier, Khumbu Himal, Nepal. *Journal of Glaciology*, *47*(159), 626-638.
- **Benn**, D. I., Warren, C. R., & Mottram, R. H. (2007). Calving processes and the dynamics of calving glaciers. *Earth-Science Reviews*, *82*(3-4), 143-179.
- **Benn**, D., Gulley, J., Luckman, A., Adamek, A., & Glowacki, P. S. (2009). Englacial drainage systems formed by hydrologically driven crevasse propagation. *Journal of Glaciology*, *55*(191), 513-523.
- **Benn**, D. I., Bolch, T., Hands, K., Gulley, J., Luckman, A., Nicholson, L. I., ... & Wiseman, S. (2012). Response of debris-covered glaciers in the Mount Everest region to recent warming, and implications for outburst flood hazards. *Earth-Science Reviews*, *114*(1-2), 156-174.
- **Bhattacharya**, A., Mukherjee, K., King, O., Karmakar, S., Remya, S. N., Kulkarni, A. V., ... & Bolch, T. (2023). Influence of climate and non-climatic attributes on declining glacier mass budget and surging in Alaknanda Basin and its surroundings. *Global and Planetary Change*, *230*, 104260.
- **Böhner**, J. (2006). General climatic controls and topoclimatic variations in Central and High Asia. *Boreas*, *35*(2), 279-295.
- **Bolch**, T., Kulkarni, A., Kääb, A., Huggel, C., Paul, F., Cogley, J. G., ... & Stoffel, M. (2012). The state and fate of Himalayan glaciers. *Science*, *336*(6079), 310-314.
- **Bookhagen**, B., & Burbank, D. W. (2010). Toward a complete Himalayan hydrological budget: Spatiotemporal distribution of snowmelt and rainfall and their impact on river discharge. *Journal of Geophysical Research: Earth Surface*, *115*(F3).
- **Boyce**, E. S., Motyka, R. J., & Truffer, M. (2007). Flotation and retreat of a lake-calving terminus, Mendenhall Glacier, southeast Alaska, USA. *Journal of Glaciology*, *53*(181), 211-224.
- **Carrivick**, J. L., & Tweed, F. S. (2013). Proglacial lakes: character, behaviour and geological importance. *Quaternary Science Reviews*, *78*, 34-52.
- **Carrivick**, J. L., & Tweed, F. S. (2016). A global assessment of the societal impacts of glacier outburst floods. *Global and Planetary Change*, *144*, 1-16.
- **Clague**, J. J., & O'Connor, J. E. (2021). Glacier-related outburst floods. In *Snow and ice-related hazards, risks, and disasters* (pp. 467-499). Elsevier.
- **Colgan**, W., Rajaram, H., Abdalati, W., McCutchan, C., Mottram, R., Moussavi, M. S., & Grigsby, S. (2016). Glacier crevasses: Observations, models, and mass balance implications. *Reviews of Geophysics*, *54*(1), 119-161.
- **Dehecq**, A., Gourmelen, N., Gardner, A. S., Brun, F., Goldberg, D., Nienow, P. W., ... & Trouvé, E. (2019). Twenty-first century glacier slowdown driven by mass loss in High Mountain Asia. *Nature Geoscience*, *12*(1), 22-27.
- **Dupont**, T. K., & Alley, R. B. (2005). Assessment of the importance of ice-shelf buttressing to ice-sheet flow. *Geophysical Research Letters*, *32*(4).
- **Farinotti**, D., Round, V., Huss, M., Compagno, L., & Zekollari, H. (2019*a*). Large hydropower and water-storage potential in future glacier-free basins. *Nature*, *575*(7782), 341-344.
- **Farinotti**, D., Huss, M., Fürst, J. J., Landmann, J., Machguth, H., Maussion, F., & Pandit, A. (2019*b*). A consensus estimate for the ice thickness distribution of all glaciers on Earth. *Nature Geoscience*, *12*(3), 168-173.
- **Fowler**, A., & Ng, F. (Eds.). (2021). *Glaciers and Ice Sheets in the climate system: The Karthaus summer school lecture notes.* Springer Nature.
- **Fujita**, K., Sakai, A., Nuimura, T., Yamaguchi, S., & Sharma, R. R. (2009). Recent changes in Imja Glacial Lake and its damming moraine in the Nepal Himalaya revealed by in situ surveys and multi-temporal ASTER imagery. *Environmental Research Letters*, *4*(4), 045205.
- **Furian**, Wilhelm (2020): An inventory of future glacial lakes in High Mountain Asia in shapefile format, v0.1, *Zenodo*, DOI: 10.5181/zenodo.3958786
- **Furian**, W., Loibl, D., & Schneider, C. (2021). Future glacial lakes in High Mountain Asia: an inventory and assessment of hazard potential from surrounding slopes. *Journal of Glaciology*, *67*(264), 653-670.
- **Furian**, W., Maussion, F., & Schneider, C. (2022). Projected 21st-century glacial lake evolution in High Mountain Asia.
- **Gardelle**, J., Arnaud, Y., & Berthier, E. (2011). Contrasted evolution of glacial lakes along the Hindu Kush Himalaya mountain range between 1990 and 2009. *Global and Planetary Change*, *75*(1-2), 47-55.
- **Gardner**, A. S., Moholdt, G., Cogley, J. G., Wouters, B., Arendt, A. A., Wahr, J., ... & Paul, F. (2013). A reconciled estimate of glacier contributions to sea level rise: 2003 to 2009. *science*, *340*(6134), 852-857.
- **Geirsdóttir**, Á., Miller, G. H., Wattrus, N. J., Björnsson, H., & Thors, K. (2008). Stabilization of glaciers terminating in closed water bodies: Evidence and broader implications. *Geophysical Research Letters*, *35*(17).
- **Gledhill**, L. A., & Williamson, A. G. (2018). Inland advance of supraglacial lakes in north-west Greenland under recent climatic warming. *Annals of Glaciology*, *59*(76pt1), 66-82.
- **Guillet**, G., King, O., Lv, M., Ghuffar, S., Benn, D., Quincey, D., & Bolch, T. (2022). A regionally resolved inventory of High Mountain Asia surge-type glaciers, derived from a multi-factor remote sensing approach. *The Cryosphere*, *16*(2), 603-623.
- **Gulley**, J., & Benn, D. I. (2007). Structural control of englacial drainage systems in Himalayan debris-covered glaciers. *Journal of Glaciology*, *53*(182), 399-412.
- **Hanshaw**, M. N., & Bookhagen, B. (2014). Glacial areas, lake areas, and snow lines from 1975 to 2012: status of the Cordillera Vilcanota, including the Quelccaya Ice Cap, northern central Andes, Peru. *The Cryosphere*, *8*(2), 359-376.

- **Haritashya**, U. K., Kargel, J. S., Shugar, D. H., Leonard, G. J., Strattman, K., Watson, C. S., ... & Regmi, D. (2018). Evolution and controls of large glacial lakes in the Nepal Himalaya. *Remote Sensing*, *10*(5), 798.
- **Heid**, T., & Kääb, A. (2012). Evaluation of existing image matching methods for deriving glacier surface displacements globally from optical satellite imagery. *Remote Sensing of Environment*, *118*, 339-355.
- **Herzfeld**, U. C., Clarke, G. K., Mayer, H., & Greve, R. (2004). Derivation of deformation characteristics in fast-moving glaciers. *Computers & Geosciences*, *30*(3), 291-302.
- **Hock**, R., Bliss, A., Marzeion, B. E. N., Giesen, R. H., Hirabayashi, Y., Huss, M., ... & Slangen, A. B. (2019). GlacierMIP–A model intercomparison of global-scale glacier mass-balance models and projections. *Journal of Glaciology*, *65*(251), 453-467.
- **Huss**, M. (2013). Density assumptions for converting geodetic glacier volume change to mass change. *The Cryosphere*, *7*(3), 877-887.
- **IPCC**, 2021: *Climate Change 2021: The Physical Science Basis. Contribution of Working Group I to the Sixth Assessment Report of the Intergovernmental Panel on Climate Change*[Masson-Delmotte, V., P. Zhai, A. Pirani, S.L. Connors, C. Péan, S. Berger, N. Caud, Y. Chen, L. Goldfarb, M.I. Gomis, M. Huang, K. Leitzell, E. Lonnoy, J.B.R. Matthews, T.K. Maycock, T. Waterfield, O. Yelekçi, R. Yu, and B. Zhou (eds.)]. Cambridge University Press, Cambridge, United Kingdom and New York, NY, USA.
- **Ji**, L., Zhang, L., & Wylie, B. (2009). Analysis of dynamic thresholds for the normalized difference water index. *Photogrammetric Engineering & Remote Sensing*, *75*(11), 1307-1317.
- **Jiang**, S., Nie, Y., Liu, Q., Wang, J., Liu, L., Hassan, J., ... & Xu, X. (2018). Glacier change, supraglacial debris expansion and glacial lake evolution in the Gyirong river basin, central Himalayas, between 1988 and 2015. *Remote Sensing*, *10*(7), 986.
- **Jiskoot**, H. (2011). Dynamics of glaciers. *physical Research*, *92*(B9), 9083-9100.
- **Kääb**, A. (2005). Combination of SRTM3 and repeat ASTER data for deriving alpine glacier flow velocities in the Bhutan Himalaya. *Remote Sensing of Environment*, *94*(4), 463-474.
- **Kääb**, A., Winsvold, S. H., Altena, B., Nuth, C., Nagler, T., & Wuite, J. (2016). Glacier remote sensing using Sentinel-2. Part I: Radiometric and geometric performance, and application to ice velocity. *Remote sensing*, *8*(7), 598.
- **Khadka**, N., Chen, X., Sharma, S., & Shrestha, B. (2023). Climate change and its impacts on glaciers and glacial lakes in Nepal Himalayas. *Regional Environmental Change*, *23*(4), 143.
- **King**, O., Bhattacharya, A., Bhambri, R., & Bolch, T. (2019). Glacial lakes exacerbate Himalayan glacier mass loss. *Scientific Reports*, *9*(1), 18145.
- **Kirkbride**, M. P., & Warren, C. R. (1999). Tasman Glacier, New Zealand: 20th-century thinning and predicted calving retreat. *Global and Planetary Change*, *22*(1-4), 11-28.
- **Komori**, J. (2008). Recent expansions of glacial lakes in the Bhutan Himalayas. *Quaternary International*, *184*(1), 177-186.
- **Kraaijenbrink**, P. D., Bierkens, M. F. P., Lutz, A. F., & Immerzeel, W. W. (2017). Impact of a global temperature rise of 1.5 degrees Celsius on Asia's glaciers. *Nature*, *549*(7671), 257-260.
- **Kulkarni**, A. V., Shirsat, T. S., Kulkarni, A., Negi, H. S., Bahuguna, I. M., & Thamban, M. (2021). State of Himalayan cryosphere and implications for water security. *Water Security*, *14*, 100101.
- **Leeson**, A. A., Shepherd, A., Briggs, K., Howat, I., Fettweis, X., Morlighem, M., & Rignot, E. (2015). Supraglacial lakes on the Greenland ice sheet advance inland under warming climate. *Nature Climate Change*, *5*(1), 51-55.
- **Lesi**, M., Nie, Y., Shugar, D. H., Wang, J., Deng, Q., Chen, H., & Fan, J. (2022). Landsat-and Sentinel-derived glacial lake dataset in the China–Pakistan Economic Corridor from 1990 to 2020. *Earth System Science Data*, *14*(12), 5489-5512.
- **Luckman**, A., Quincey, D., & Bevan, S. (2007). The potential of satellite radar interferometry and feature tracking for monitoring flow rates of Himalayan glaciers. *Remote sensing of Environment*, *111*(2-3), 172-181.
- **Marshall**, S. J. (2011). *The cryosphere* (Vol. 4). Princeton University Press.
- **Marzeion**, B., Hock, R., Anderson, B., Bliss, A., Champollion, N., Fujita, K., ... & Zekollari, H. (2020). Partitioning the uncertainty of ensemble projections of global glacier mass change. *Earth's Future*, *8*(7), e2019EF001470.
- **Maurer**, J., S. Rupper, and J. Schaefer. (2019). High Mountain Asia Glacier Thickness Change Mosaics from Multi-Sensor DEMs, Version 1 [Data Set]. Boulder, Colorado USA. NASA National Snow and Ice Data Center Distributed Active Archive Center.
- **Mertes**, J. R., Thompson, S. S., Booth, A. D., Gulley, J. D., & Benn, D. I. (2017). A conceptual model of supra-glacial lake formation on debris-covered glaciers based on GPR facies analysis. *Earth Surface Processes and Landforms*, *42*(6), 903-914.
- **Millan**, R., Mouginot, J., Rabatel, A., & Morlighem, M. (2022). Ice velocity and thickness of the world's glaciers. *Nature Geoscience*, *15*(2), 124-129.
- **Minowa**, M., Schaefer, M., & Skvarca, P. (2023). Effects of topography on dynamics and mass loss of lake-terminating glaciers in southern Patagonia. *Journal of Glaciology*, 1-18.
- **Motyka**, R. J., Hunter, L., Echelmeyer, K. A., & Connor, C. (2003). Submarine melting at the terminus of a temperate tidewater glacier, LeConte Glacier, Alaska, USA. *Annals of Glaciology*, *36*, 57-65.
- **Nagy**, T., & Andreassen, L. (2019). Glacier lake mapping with Sentinel-2 imagery in Norway. *NVE Rapport*, 40-2019.
- **Nick**, F. M., Vieli, A., Andersen, M. L., Joughin, I., Payne, A., Edwards, T. L., ... & van de Wal, R. S. (2013). Future sea-level rise from Greenland's main outlet glaciers in a warming climate. *Nature*, *497*(7448), 235-238.
- **Otto**, J. C., Helfricht, K., Prasicek, G., Binder, D., & Keuschnig, M. (2022). Testing the performance of ice thickness models to estimate the formation of potential future glacial lakes in Austria. *Earth Surface Processes and Landforms*, *47*(3), 723-741.
- **Pratap**, B., Dobhal, D. P., Mehta, M., & Bhambri, R. (2015). Influence of debris cover and altitude on glacier surface melting: a case study on Dokriani Glacier, central Himalaya, India. *Annals of Glaciology*, *56*(70), 9-16.
- **Pronk**, J. B., Bolch, T., King, O., Wouters, B., & Benn, D. I. (2021). Contrasting surface velocities between lake-and land-terminating glaciers in the Himalayan region. *The Cryosphere*, *15*(12), 5577-5599.
- **Qayyum**, N., Ghuffar, S., Ahmad, H. M., Yousaf, A., & Shahid, I. (2020). Glacial lakes mapping using multi satellite PlanetScope imagery and deep learning. *ISPRS International Journal of Geo-Information*, *9*(10), 560.
- **Quincey**, D. J., Luckman, A., & Benn, D. (2009). Quantification of Everest region glacier velocities between 1992 and 2002, using satellite radar interferometry and feature tracking. *Journal of Glaciology*, *55*(192), 596-606.
- **RGI Consortium**. (2023). Randolph Glacier Inventory - A Dataset of Global Glacier Outlines, Version 7.0. Boulder, Colorado USA. NSIDC: National Snow and Ice Data Center. doi:10.5067/f6jmovy5navz.
- **Rinzin**, S., Zhang, G., & Wangchuk, S. (2021). Glacial lake area change and potential outburst flood hazard assessment in the Bhutan Himalaya. *Frontiers in Earth Science*, 1136.

- **Rinzin**, S., Zhang, G., Sattar, A., Wangchuk, S., Allen, S. K., Dunning, S., & Peng, M. (2023). GLOF hazard, exposure, vulnerability, and risk assessment of potentially dangerous glacial lakes in the Bhutan Himalaya. *Journal of Hydrology*, *619*, 129311.
- **Röhl**, K. (2006). Thermo-erosional notch development at fresh-water-calving Tasman Glacier, New Zealand. *Journal of Glaciology*, *52*(177), 203-213.
- **Röhl**, K. (2008). Characteristics and evolution of supraglacial ponds on debris-covered Tasman Glacier, New Zealand. *Journal of Glaciology*, *54*(188), 867-880.
- **Rowan**, A. V., Egholm, D. L., Quincey, D. J., Hubbard, B., King, O., Miles, E. S., ... & Hornsey, J. (2021). The role of differential ablation and dynamic detachment in driving accelerating mass loss from a debris-covered Himalayan glacier. *Journal of Geophysical Research: Earth Surface*, *126*(9), e2020JF005761.
- **Sakai**, A., Takeuchi, N., Fujita, K., & Nakawo, M. (2000). Role of supraglacial ponds in the ablation process of a debris-covered glacier in the Nepal Himalayas. *Iahs publication*, 119-132.
- **Sakai**, A., Nishimura, K., Kadota, T., & Takeuchi, N. (2009). Onset of calving at supraglacial lakes on debris-covered glaciers of the Nepal Himalaya. *Journal of Glaciology*, *55*(193), 909-917.
- **Sakai**, A., & Fujita, K. (2017). Contrasting glacier responses to recent climate change in high-mountain Asia. *Scientific reports*, *7*(1), 13717.
- **Sato**, Y., Fujita, K., Inoue, H., & Sakai, A. (2022). Land-to lake-terminating transition triggers dynamic thinning of a Bhutanese glacier. *The Cryosphere*, *16*(6), 2643-2654.
- **Scherler**, D., Bookhagen, B., & Strecker, M. R. (2011). Hillslope-glacier coupling: The interplay of topography and glacial dynamics in High Asia. *Journal of Geophysical Research: Earth Surface*, *116*(F2).
- **Shean**, D. (2017). High Mountain Asia 8-meter DEM Mosaics Derived from Optical Imagery, Version 1 [Data Set]. Boulder, Colorado USA. NASA National Snow and Ice Data Center Distributed Active Archive Center.
- **Shean**, D. E., Bhushan, S., Montesano, P., Rounce, D. R., Arendt, A., & Osmanoglu, B. (2020). A systematic, regional assessment of high mountain Asia glacier mass balance. *Frontiers in Earth Science*, *7*, 363.
- **Shugar**, D. H., Burr, A., Haritashya, U. K., Kargel, J. S., Watson, C. S., Kennedy, M. C., ... & Strattman, K. (2020). Rapid worldwide growth of glacial lakes since 1990. *Nature Climate Change*, *10*(10), 939-945.
- **Singh**, S. M. (2009). The Cost of Climate Change: The Story of Thorthormi Glacial Lake in Bhutan. *WWF: Gland, Switzerland*, 1-32.
- **Song**, C., Sheng, Y., Ke, L., Nie, Y., & Wang, J. (2016). Glacial lake evolution in the southeastern Tibetan Plateau and the cause of rapid expansion of proglacial lakes linked to glacial-hydrogeomorphic processes. *Journal of hydrology*, *540*, 504-514.
- **Stokes**, C. R., Sanderson, J. E., Miles, B. W., Jamieson, S. S., & Leeson, A. A. (2019). Widespread distribution of supraglacial lakes around the margin of the East Antarctic Ice Sheet. *Scientific reports*, *9*(1), 13823.
- **Tedesco**, M. (2015). Remote sensing and the cryosphere. *Remote Sensing of the Cryosphere*, 1-16.
- **Truffer**, M., & Motyka, R. J. (2016). Where glaciers meet water: Subaqueous melt and its relevance to glaciers in various settings. *Reviews of Geophysics*, *54*(1), 220-239.
- **Tsutaki**, S., Sugiyama, S., Nishimura, D., & Funk, M. (2013). Acceleration and flotation of a glacier terminus during formation of a proglacial lake in Rhonegletscher, Switzerland. *Journal of Glaciology*, *59*(215), 559-570.
- **Tsutaki**, S., Fujita, K., Nuimura, T., Sakai, A., Sugiyama, S., Komori, J., & Tshering, P. (2019). Contrasting thinning patterns between lake-and land-terminating glaciers in the Bhutanese Himalaya. *The Cryosphere*, *13*(10), 2733-2750.
- **Tweed**, F. S., & Carrivick, J. L. (2015). Deglaciation and proglacial lakes. *Geology Today*, *31*(3), 96-102.
- **Van der Veen**, C. J. (1998). Fracture mechanics approach to penetration of surface crevasses on glaciers. *Cold Regions Science and Technology*, *27*(1), 31-47.
- **Van Huizen**, J.P. (2024). Testing different calving parametrizations for describing calving processes inside proglacial lakes in the Himalayan region using Open Global Glacier Model [Unpublished manuscript].
- **Van Wyk de Vries**, M. (2021*a*). Glacier Image Velocimetry (GIV) App, https://doi.org/10.5281/zenodo.4147589.
- **Van Wyk de Vries**, M. (2021*b*). Glacier Image Velocimetry (GIV) User Manual V1.0.
- **Van Wyk de Vries**, M., & Wickert, A. D. (2021). Glacier Image Velocimetry: an open-source toolbox for easy and rapid calculation of high-resolution glacier velocity fields. *The Cryosphere*, *15*(4), 2115-2132.
- **Veettil**, B. K., Bianchini, N., de Andrade, A. M., Bremer, U. F., Simões, J. C., & de Souza Junior, E. (2016). Glacier changes and related glacial lake expansion in the Bhutan Himalaya, 1990–2010. *Regional environmental change*, *16*, 1267-1278.
- **Wangchuk**, S., Bolch, T., & Robson, B. A. (2022). Monitoring glacial lake outburst flood susceptibility using Sentinel-1 SAR data, Google Earth Engine, and persistent scatterer interferometry. *Remote Sensing of Environment*, *271*, 112910.
- **Watanbe**, T., & Rothacher, D. (1996). The 1994 Lugge Tsho glacial lake outburst flood, Bhutan Himalaya. *Mountain Research and Development*, *16*(1), 77-81.
- **Watson**, C. S., King, O., Miles, E. S., & Quincey, D. J. (2018). Optimising NDWI supraglacial pond classification on Himalayan debris-covered glaciers. *Remote sensing of environment*, *217*, 414-425.
- **Wendleder**, A., Friedl, P., & Mayer, C. (2018). Impacts of climate and supraglacial lakes on the surface velocity of Baltoro Glacier from 1992 to 2017. *Remote Sensing*, *10*(11), 1681.
- **Wendleder**, A., Schmitt, A., Erbertseder, T., D'Angelo, P., Mayer, C., & Braun, M. H. (2021). Seasonal evolution of supraglacial lakes on Baltoro Glacier from 2016 to 2020. *Frontiers in Earth Science*, *9*, 725394.
- **Zhang**, G., Yao, T., Xie, H., Wang, W., & Yang, W. (2015). An inventory of glacial lakes in the Third Pole region and their changes in response to global warming. *Global and Planetary Change*, *131*, 148-157.
- **Zhang**, G., Bolch, T., Yao, T., Rounce, D. R., Chen, W., Veh, G., ... & Wang, W. (2023). Underestimated mass loss from lake-terminating glaciers in the greater Himalaya. *Nature Geoscience*, *16*(4), 333-338.
- **Zheng**, G., Allen, S. K., Bao, A., Ballesteros-Cánovas, J. A., Huss, M., Zhang, G., ... & Stoffel, M. (2021). Increasing risk of glacial lake outburst floods from future Third Pole deglaciation. *Nature Climate Change*, 11(5), 411-417.

Appendix

Date	*Satellite*	*Path/Row*	*# Scenes*	*Instrument type*	*Grid size (m)*	*Green/NIR bands*	*NDWI threshold*
2003-11-18	Landsat 4-5	138/40	1	TM	30	2/4	0.11
2004-10-19	Landsat 4-5	138/40	1	TM	30	2/4	0.13
2005-11-07	Landsat 4-5	138/40	1	TM	30	2/4	0.13
2006-10-25	Landsat 4-5	138/40	1	TM	30	2/4	0.13
2008-12-17	Landsat 4-5	138/40	1	TM	30	2/4	0.13
2009-11-09	RapidEye		2	RapidEye-3	6.5	2/5	0.34
2010-11-05	RapidEye		1	RapidEye-1	6.5	2/5	0.30
2012-10-17	RapidEye		1	RapidEye-3	6.5	2/5	0.34
2013-11-24	RapidEye		1	RapidEye-1	6.5	2/5	0.32
2014-11-26	RapidEye		1	RapidEye-2	6.5	2/5	0.34
2015-11-13	RapidEye		1	RapidEye-2	6.5	2/5	0.34
2016-12-16	PlanetScope		13	PS2	3	2/4	0.36
2017-11-19	PlanetScope		10	PS2	3	2/4	0.37
2018-12-02	PlanetScope		11	PS2	3	2/4	0.34
2019-11-27	PlanetScope		11	PS2/PS2.SD	3	2/4	0.38
2020-10-24	PlanetScope		16	PS2/PS2.SD/PSB.SD	3	2/4	0.38
2021-11-08	PlanetScope		9	PS2/PSB.SD	3	2/4	0.38
2022-10-19	PlanetScope		10	PSB.SD	3	2/4	0.38
2023-10-25	PlanetScope		5	PSB.SD	3	2/4	0.38

Tab. A1. *Overview of the selected satellite images for mapping the spatiotemporal evolution of glacial lakes. Incorporated are the satellite-specific bands inserted in the NDWI equation. Note that the NDWI threshold can differ slightly for the same satellite.*

	2022 (PlanetScope)		*2020 (PlanetScope)*		*2017 (PlanetScope)*		*2013-2014 (LS8-9)*		*2006-2007 (LS4-5)*	
Glaciers	Timespan	#images	Timespan	#images	Timespan	#images	Timespan	#images	Timespan	#images
Lugge	05/08-24/12	13	07/08-23/12	12	29/08-30/12	11	25/08-01/02	7	22/08-29/01	8
Thorthormi	09/08-23-12	12	04/08-27/12	14	29/08-30/12	11	25/08-01/02	7	22/08-29/01	8
Raphsthreng	05/08-23/12	11	04/08-30/12	16	19/09-28/12	12	25/08-01/02	7	22/08-29/01	8
Bechung	05/08-24/12	14	04/08-22/12	15	26/08-23/12	13	25/08-01/02	7	22/08-29/01	8
G528	05/08-22/12	14	20/08-28/12	13	26/08-28/12	15	25/08-01/02	7	22/08-29/01	8

Tab. A2. *Overview of the selected time periods and the corresponding number of images for the selected glaciers. These images were used as input in the feature tracking tool.*

Glacier front (m)	**2000**	**2006**	**2013**	**2017**	**2020**	**2022**
G528	-	-	-	-	-	-
Bechung	6035	5544	5038	4837	4698	4563
Raphsthreng	2616	2538	2485	2332	2434	2155
Thorthormi	7036	7036	5733	4226	4525	2761
Lugge	4861	4503	3951	3720	3535	3438

Tab. A3. *The estimated calving front (in m) for each glacier along the flowline derived from satellite imagery. These values were implemented in the flow velocity and thinning rate graphs to filter out values exceeding the glacier boundary for the specific year.*

Year	Grid Size (m)	Area (m²)	Perimeter (m)	Error (σ)	Relative Error (%)
2003	30	73800	3084	31789,872	43,07570732
2004	30	80639	2974	30655,992	38,01633453
2005	30	103899	3123	32191,884	30,98382468
2006	30	100164	3591	37016,028	36,95542111
2008	30	170997	2376	24491,808	14,32294602
2009	6,5	211850	3063	6840,9042	3,229126363
2010	6,5	229497	3093	6907,9062	3,010020262
2012	6,5	250281	3111	6948,1074	2,776122598
2013	6,5	279327	3352	7486,3568	2,680140767
2014	6,5	296376	3511	7841,4674	2,645783532
2015	6,5	323644	3485	7783,399	2,404926092
2016	3	345053	3652	3764,4816	1,090986486
2017	3	368406	3770	3886,116	1,054846012
2018	3	394034	3881	4000,5348	1,01527655
2019	3	409286	4125	4252,05	1,038894563
2020	3	411421	4075	4200,51	1,02097608
2021	3	443590	4362	4496,3496	1,013627359
2022	3	476886	4361	4495,3188	0,942640128
2023	3	480445	4277	4408,7316	0,917635026

Tab. A4.1. *The lake detection data for the Bechung glacier imported in* ***fig. 7****. The relative error is the deviation in percentages from the area.*

Year	Grid Size (m)	Area (m²)	Perimeter (m)	Error (σ)	Relative Error (%)
2003	30	1224045	4968	51210,144	4,183681482
2004	30	1210070	4958	51107,064	4,223479964
2005	30	1233221	4994	51478,152	4,174284415
2006	30	1222595	4991	51447,228	4,208035204
2008	30	1243105	5380	55457,04	4,461171019
2009	6,5	1248081	5399	12058,1266	0,966133336
2010	6,5	1225151	5524	12337,3016	1,007002533
2012	6,5	1206816	5324	11890,6216	0,985288694
2013	6,5	1280383	5734	12806,3156	1,000194129
2014	6,5	1286944	5692	12712,5128	0,987806214
2015	6,5	1262545	5725	12786,215	1,012733408
2016	3	1316901	5803	5981,7324	0,454227949
2017	3	1347342	5986	6170,3688	0,45796604
2018	3	1366234	6057	6243,5556	0,456990208
2019	3	1336907	5834	6013,6872	0,449820908
2020	3	1303580	5697	5872,4676	0,450487703
2021	3	1321993	5922	6104,3976	0,46175718
2022	3	1375455	6207	6398,1756	0,465167934
2023	3	1377339	6116	6304,3728	0,457721215

Tab. A4.2. *The lake detection data for the Raphsthreng glacier imported in* ***fig. 7****. The relative error is the deviation in percentages from the area.*

Year	Grid Size (m)	Area (m²)	Perimeter (m)	Error (σ)	Relative Error (%)
2003	30	1017305	9924	102296,592	10,05564624
2004	30	1097611	10493	108161,844	9,85429665
2005	30	1199845	11656	120150,048	10,01379745
2006	30	1234187	11985	123541,38	10,00994015
2008	30	1378014	14956	154166,448	11,18758213
2009	6,5	1449491	17414	38892,4276	2,683178274
2010	6,5	1770430	23889	53353,6926	3,013600798
2012	6,5	2249984	15590	34818,706	1,547509049
2013	6,5	2356462	16284	36368,6856	1,543359732
2014	6,5	2825107	14604	32616,5736	1,154525248
2015	6,5	2760359	14858	33183,8572	1,202157299
2016	3	2903837	15466	15942,3528	0,549009907
2017	3	3184621	16082	16577,3256	0,520543123
2018	3	3452021	15734	16218,6072	0,469829332
2019	3	3591994	14615	15065,142	0,419408885
2020	3	3698721	17093	17619,4644	0,476366409
2021	3	3840273	15741	16225,8228	0,42251743
2022	3	4249094	10615	10941,942	0,257512354
2023	3	4267058	10715	11045,022	0,258843962

Tab. A4.3. *The lake detection data for the Thorthormi glacier imported in* ***fig. 7****. The relative error is the deviation in percentages from the area.*

Year	*Grid Size (m)*	*Area (m²)*	*Perimeter (m)*	*Error (σ)*	*Relative Error (%)*
2003	30	1146094	5362	55271,496	4,822597099
2004	30	1134855	5470	56384,76	4,968455001
2005	30	1167289	5722	58982,376	5,052936848
2006	30	1183065	5594	57662,952	4,874030759
2008	30	1275827	6116	63043,728	4,941400989
2009	6,5	1351840	7599	16971,6066	1,25544492
2010	6,5	1365626	6792	15169,2528	1,110791154
2012	6,5	1411283	6942	15504,2628	1,098593464
2013	6,5	1474368	7037	15716,4358	1,065977816
2014	6,5	1479337	7247	16185,4498	1,094101601
2015	6,5	1507030	7416	16562,8944	1,099042116
2016	3	1526708	7615	7849,542	0,51414822
2017	3	1528801	7516	7747,4928	0,506769213
2018	3	1547261	7771	8010,3468	0,517711414
2019	3	1568536	7854	8095,9032	0,51614392
2020	3	1572173	8090	8339,172	0,530423306
2021	3	1611292	8192	8444,3136	0,524070969
2022	3	1635203	8167	8418,5436	0,514831712
2023	3	1657681	8303	8558,7324	0,516307565

Tab. A4.4. *The lake detection data for the Lugge glacier imported in* **fig. 7** *The relative error is the deviation in percentages from the area.*

1975-2000	*Mean dh/dt (m/yr)*	*Max dh/dt (m/yr)*	*Min dh/dt (m/yr)*	*Mass balance (m w.e./yr)*	*Mass change (Mtonnes/yr)*
G528	-0.4346	-1.8445	3.1412	-0.3694	-6.5556
Bechung	-0.0429	-1.9766	2.3052	-0.0365	-0.1274
Raphsthreng	-0.4513	-2.9176	1.1638	-0.3836	-0.7040
Thorthormi	-0.3225	-2.8179	2.8596	-0.2741	-3.1207
Lugge	-0.4192	-3.4767	2.2183	-0.3564	-2.5531

Tab. A5.1. *Statistics for the annual mean thinning rate, mass balance and mass loss per glacier between 1975 to 2000 according to Maurer et al. (2019).*

2000-2017	*Mean dh/dt (m/yr)*	*Max dh/dt (m/yr)*	*Min dh/dt (m/yr)*	*Mass balance (m w.e./yr)*	*Mass change (Mtonnes/yr)*
G528	-0.7592	-2.8075	3.4296	-0.6453	-11.3152
Bechung	-0.9881	-2.9969	0.6698	-0.8399	-3.0001
Raphsthreng	-0.7784	-2.6277	0.2772	-0.6616	-1.3369
Thorthormi	-0.6656	-4.1220	2.8653	-0.5658	-6.8453
Lugge	-0.5476	-4.1203	2.3146	-0.4655	-4.3061

Tab. A5.2. *Statistics for the annual mean thinning rate, mass balance and mass loss per glacier between 2000 to 2017 according to Maurer et al. (2019).*

2017-2022	*Mean dh/dt (m/yr)*	*Max dh/dt (m/yr)*	*Min dh/dt (m/yr)*	*Mass balance (m w.e./yr)*	*Mass change (Mtonnes/yr)*
G528	-0.9626	-15.6494	28.4847	-0.8182	-17.5658
Bechung	-1.1498	-18.5829	21.0753	-0.9773	-5.4965
Raphsthreng	-1.3464	-20.7920	43.6632	-1.1444	-2.2848
Thorthormi	-0.7658	-30.2356	51.0891	-0.6509	-6.6509
Lugge	-0.6379	-19.0404	26.0813	-0.5422	-5.2895

Tab. A5.3. *Statistics for the annual mean thinning rate, mass balance and mass loss per glacier between 2017 and 2022..*

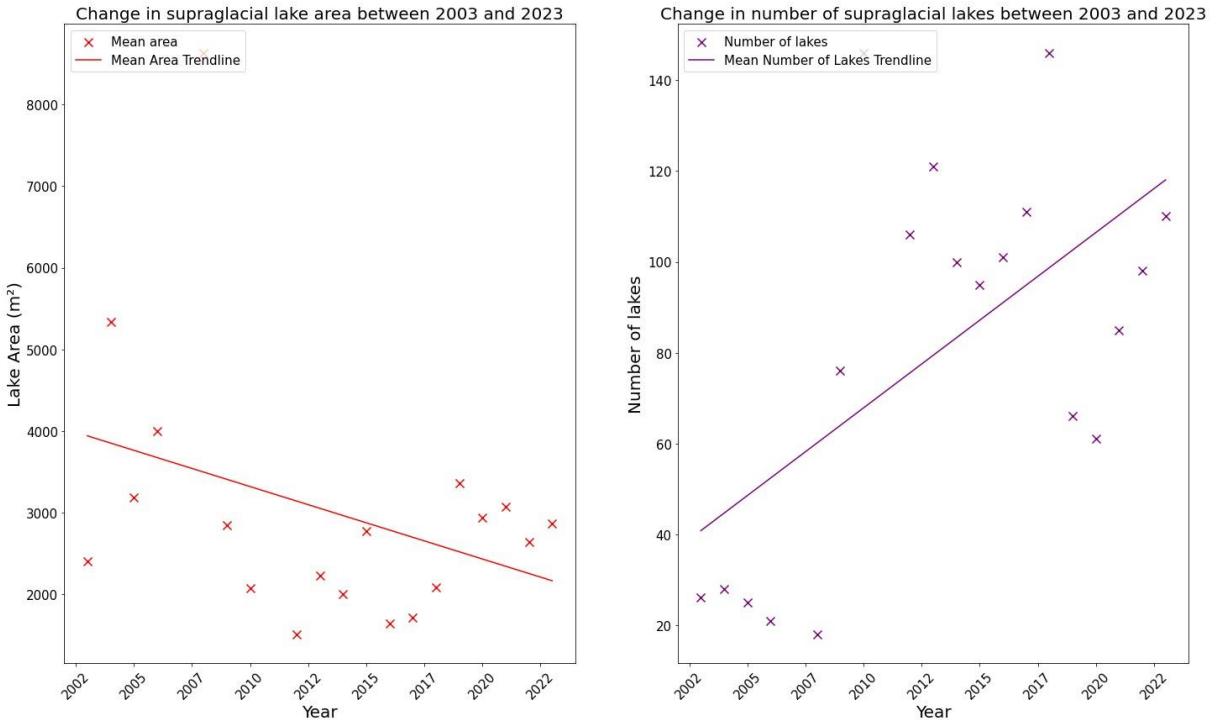

Fig. A6. *Both graphs show the trends in supraglacial lake area (left) and supraglacial lake number (right) between 2003 and 2023 on the G528 glacier, including Landsat imagery. The graphs show contrasting trends when compared to* **fig. 16***, excluding Landsat.*

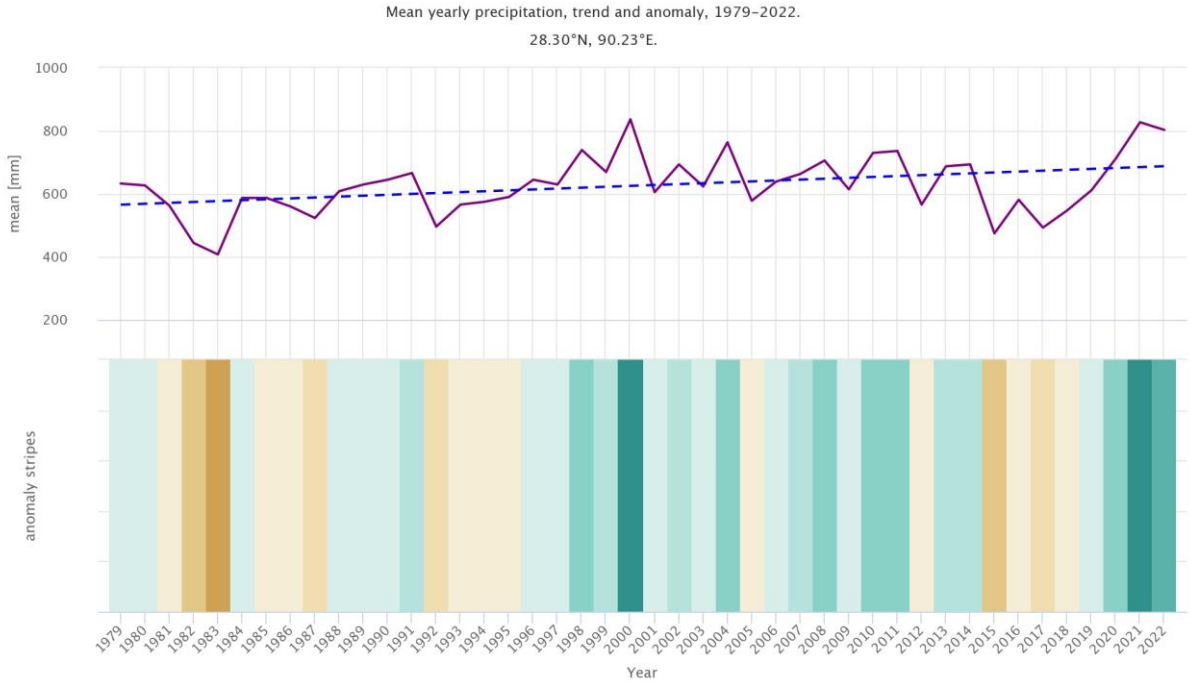

Fig. A7. *Graph showing the mean annual precipitation in the Lunana region between 1979 to 2022. The anomaly stripes present a visual interpretation of the graph of the average annual precipitation rate, where blue stripes indicate wetter periods and yellow stripes, drier periods relative to the mean [from: MeteoBlue].*

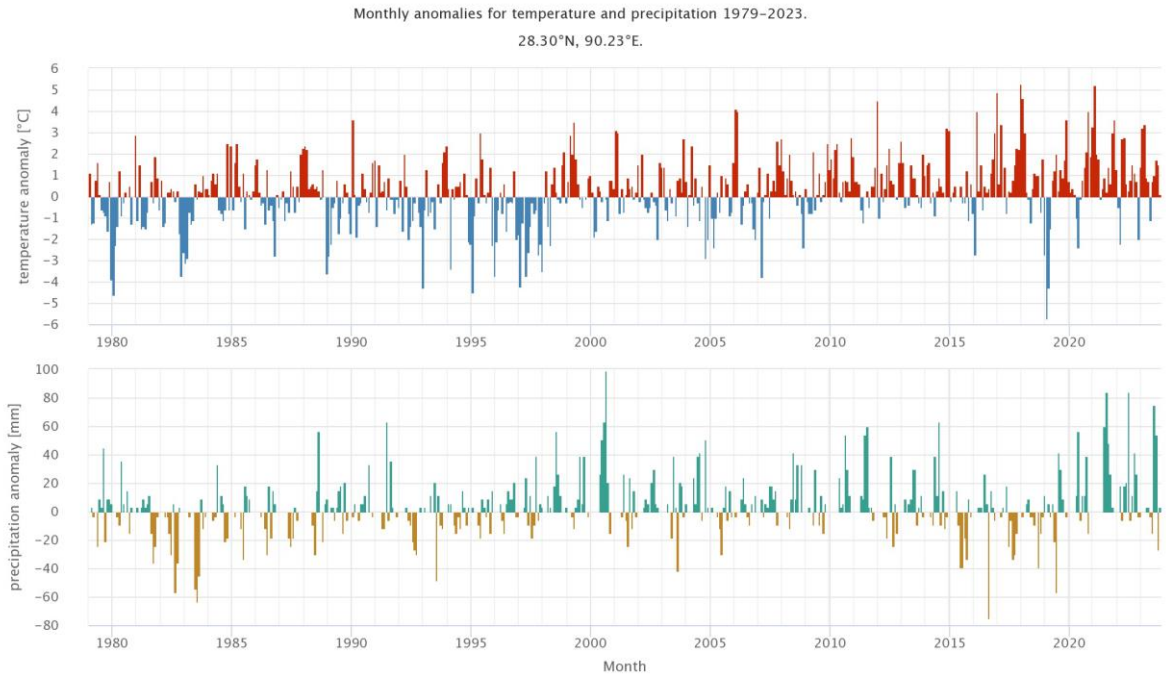

Fig. A8. *Graphs showing the monthly anomalies for temperature (upper) and precipitation (lower) in the Lunana region from 1979 to 2023. The temperature anomalies are higher in every month since 2010, except for a few specific periods. For the precipitation, the spring and summer mainly see an increase in precipitation, where autumn and winter are mainly characterized by drier spells and little changes [from: MeteoBlue].*

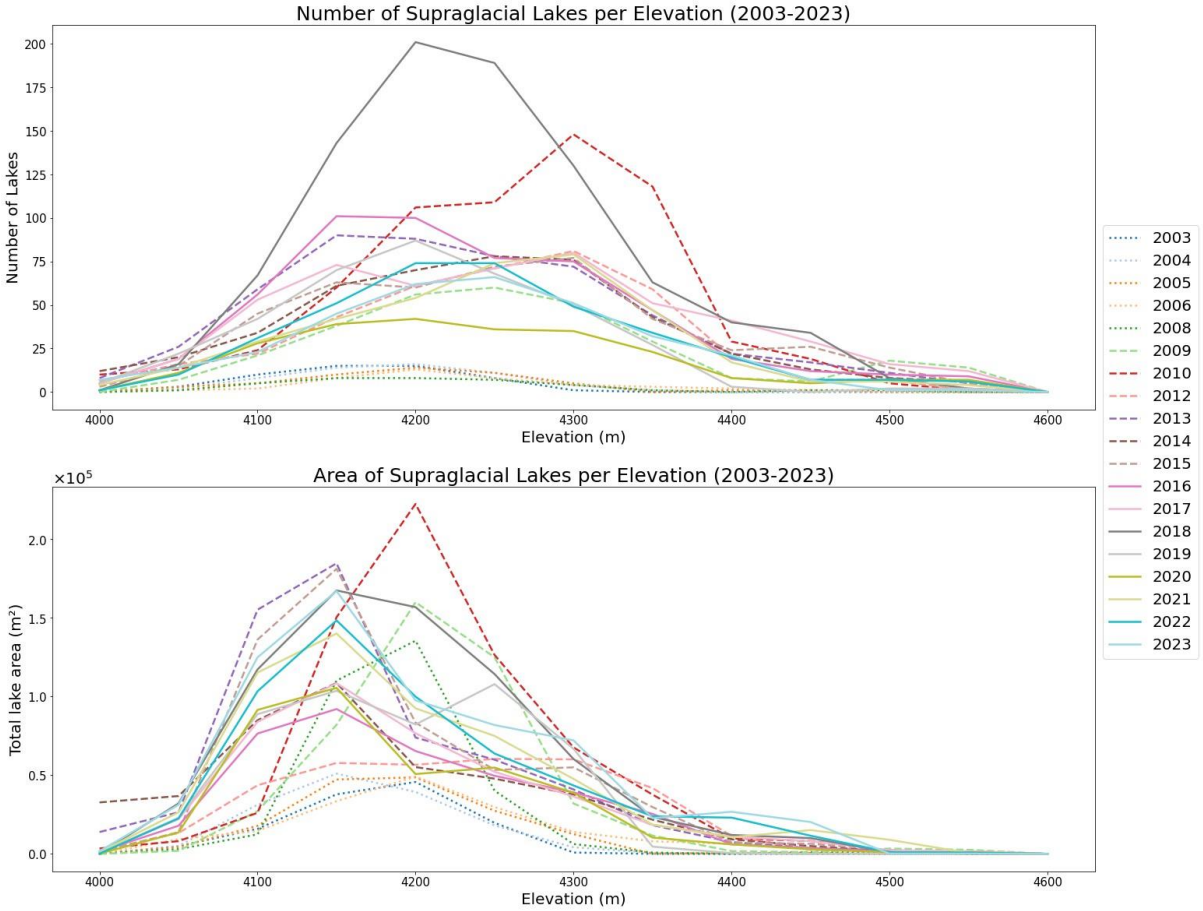

Fig. A9. *Graphs showing the number of supraglacial lakes (upper) and total area of supraglacial lakes (lower) per 50 m elevation band on the G528 glacier. The dotted lines represent Landsat, the striped lines RapidEye and solid lines PlanetScope imagery.*

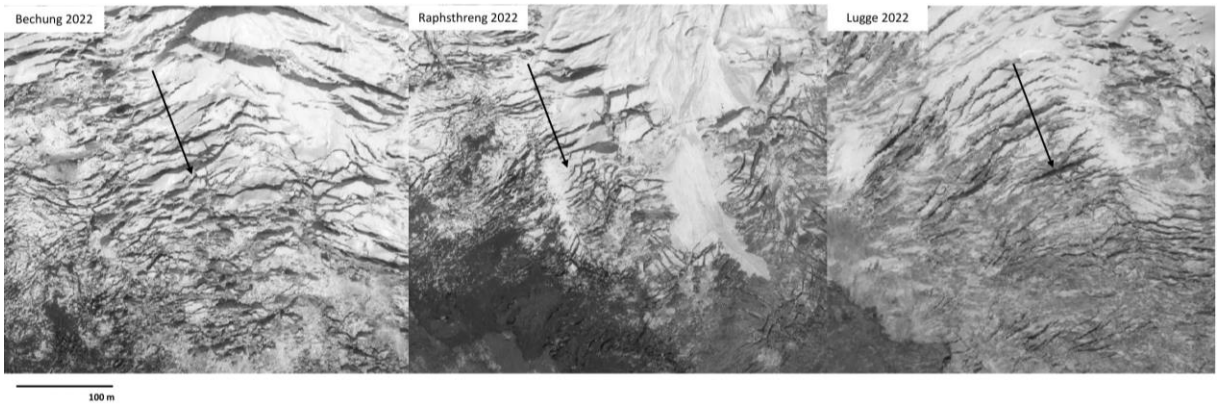

Fig. A10. *Pléiades satellite images of the upper regions of the Bechung, Raphsthreng and Lugge glacier in 2022. Highlighted are transverse crevasses forming through the stretching of the ice on the steeper slopes of the glaciers. On the sides, marginal crevasses can be observed. The arrow indicates the flow direction.*

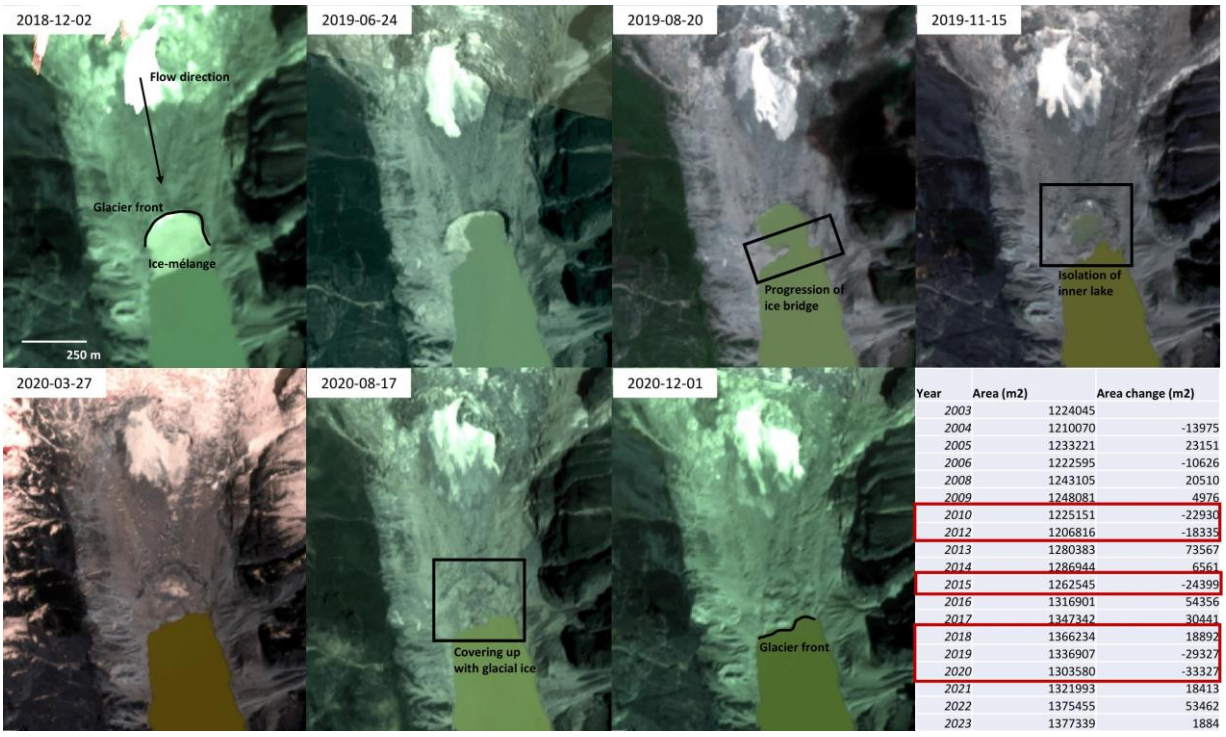

Year	Area (m2)	Area change (m2)
2003	1224045	
2004	1210070	-13975
2005	1233221	23151
2006	1222595	-10626
2008	1243105	20510
2009	1248081	4976
2010	1225151	-22930
2012	1206816	-18335
2013	1280383	73567
2014	1286944	6561
2015	1262545	-24399
2016	1316901	54356
2017	1347342	30441
2018	1366234	18892
2019	1336907	-29327
2020	1303580	-33327
2021	1321993	18413
2022	1375455	53462
2023	1377339	1884

Fig. A11. *Timeseries of PlanetScope images highlighting a glacier advance of the Raphsthreng glacier from 2018 to 2020. It is observed that an ice-bridge forms, isolating part of the lake after which it is covered by glacial ice. The table on the bottom right highlights other periods of advances.*

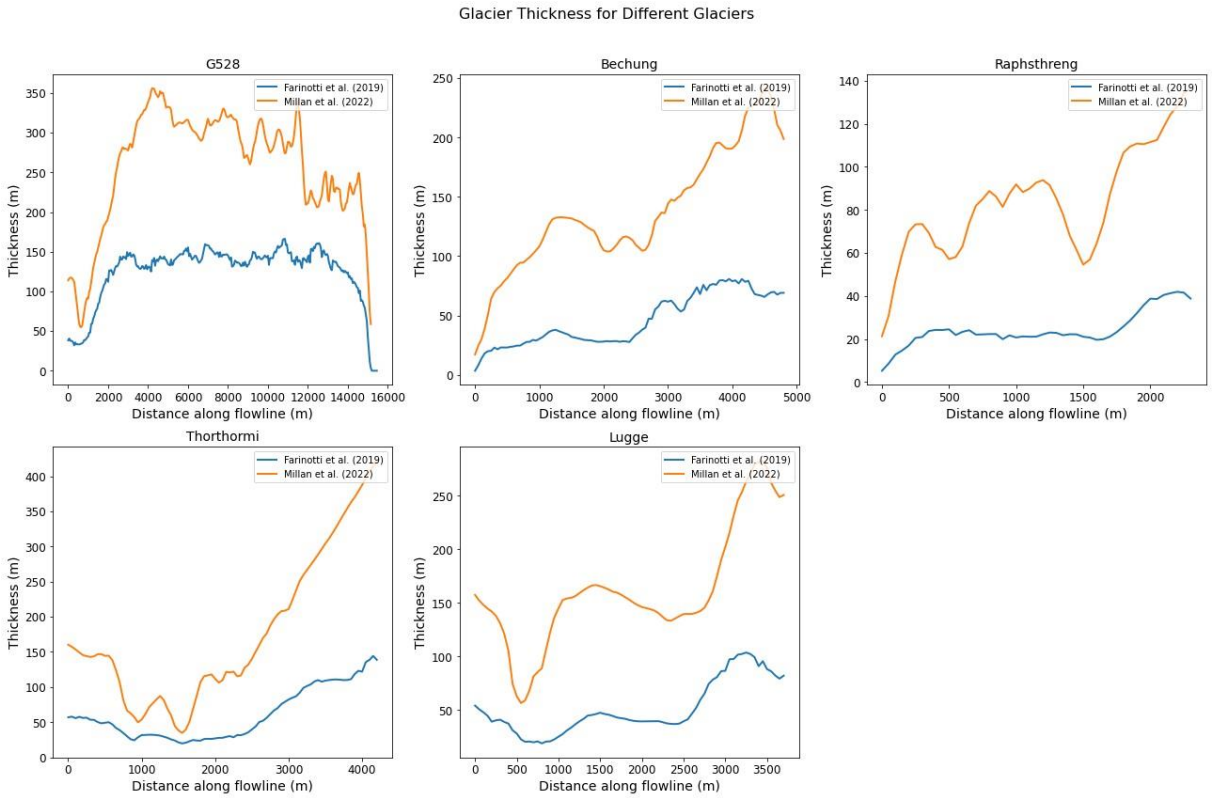

Fig. A12. *Graphs showing the modelled ice thickness of Farinotti et al. (2019) and Millan et al. (2022) for each glacier along the flowline. Both datasets show similar trends, but Millan et al. (2022) produced much higher thickness values. All glacier show the highest thickness at the terminus.*

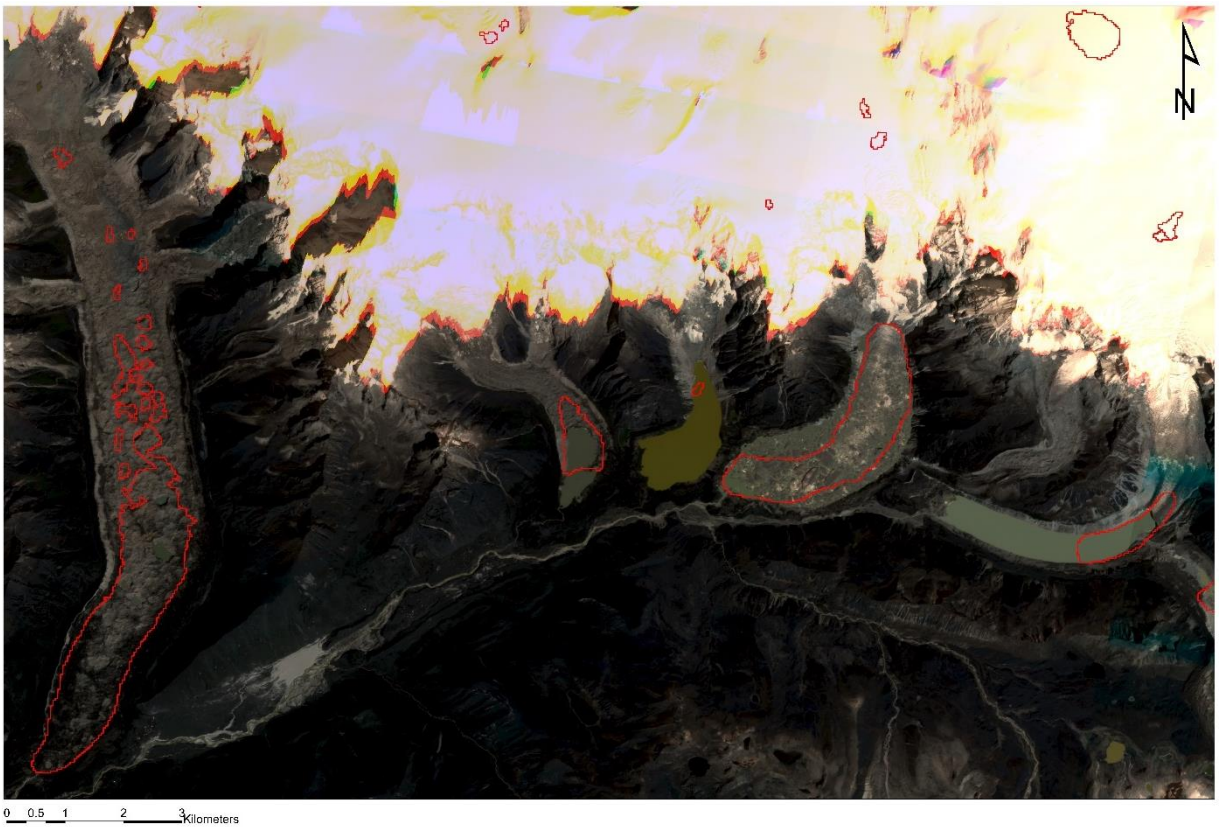

Fig. A13. *Map showing the presence of overdeepenings in the Lunana region by Furian & Wilhelm (2020), underlain by a PlanetScope image from 2022. The overdeepening of the Thorthormi is already completely filled, and the Bechung and Lugge overdeepenings are partly filled. The G528 glacier still fills the overdeepening.*

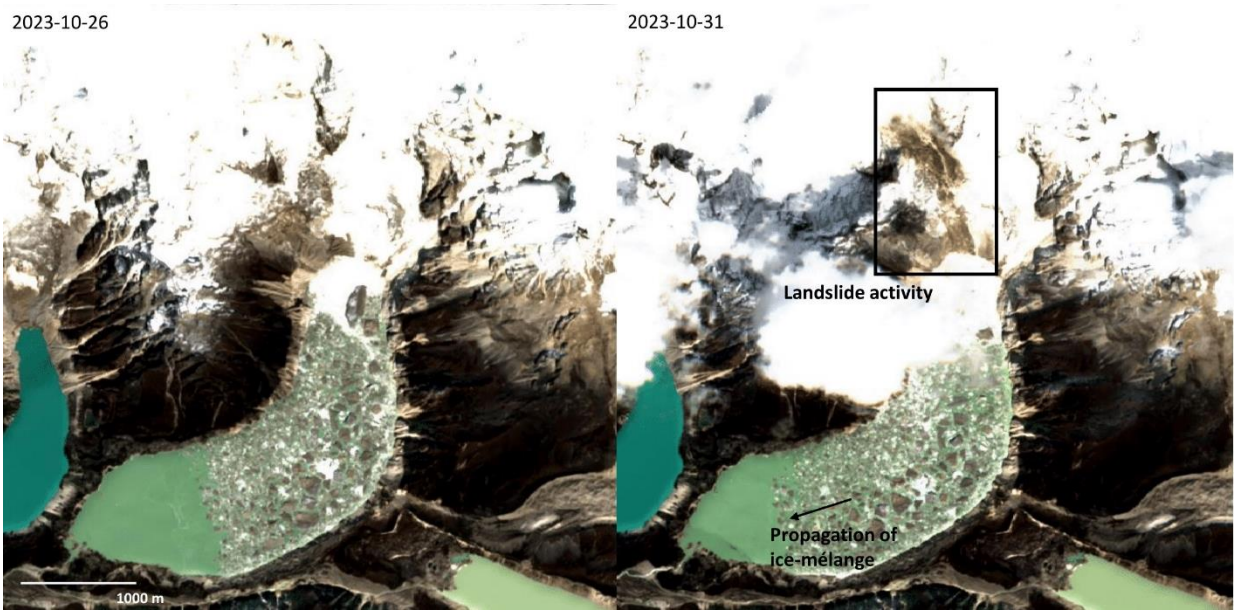

Fig. A14. *Two Sentinel-2 images showing the Thorthormi glacier before (left) and after (right) the GLOF. On the right image, the scar is visible which the ice avalanche left behind after it slid in the lake. This generated a wave which displaced the ice-mélange, indicated with the arrow. The outlet stream has slightly moved and increased discharge can be observed.*